Character count (with spacing): 39,758
Character count (without spacing): 33,457

Antagonistic relationship of NuA4 with the Non-Homologous End-Joining machinery at DNA damage sites

Salar Ahmad[1], Valerie Côté[1], Xue Cheng[1], Gaëlle Bourriquen[1], Vasileia Sapountzi[1], Mohammed Altaf[1,2] and Jacques Côté[1]#

[1] St-Patrick Research Group in Basic Oncology, Centre Hospitalier Universitaire de Québec-Université Laval Research Center, Laval University Cancer Research Center, Quebec City, QC, Canada

[2] Present address: Chromatin and Epigenetics Lab, Department of Biotechnology, University of Kashmir, Srinagar, Jammu and Kashmir 190006, India

Corresponding authors: jacques.cote@crhdq.ulaval.ca

Running Title: NuA4 curbs NHEJ favoring DNA resection

ABSTRACT

The NuA4 histone acetyltransferase complex, apart from its known role in gene regulation, has also been directly implicated in the repair of DNA double-strand breaks (DSBs), favoring homologous recombination (HR) in S/G2 during the cell cycle. Here, we investigate the antagonistic relationship of NuA4 with non-homologous end joining (NHEJ) factors. We detect NuA4 at DSBs in G1 when genes for NHEJ factors Rad9, Yku80 and Nej1 are mutated. This is accompanied with the binding of single-strand DNA binding protein RPA, indicating DNA end resection in G1. This NuA4 recruitment to DSBs depends on both Xrs2 and Lcd1/Ddc2. Introducing an acetyltransferase defective allele in these NHEJ mutant backgrounds decreases their hyper-resection phenotype in G1. Interestingly, we identified two novel non-histone acetylation targets of NuA4, Nej1 and Yku80. Acetyl-mimicking mutant of Nej1 inhibits NHEJ, decreases its interaction with other NHEJ factors and favors resection. Altogether, these results establish an antagonistic regulatory function of NuA4 and NHEJ factors in repair pathway choice and suggest a role of NuA4 in alternative repair mechanism that involves DNA-end resection in G1.

Keywords: Acetylation; double-strand break; Nej1; non-homologous end joining; NuA4

INTRODUCTION

The genomic integrity of a cell is under constant assault from various endogenous and exogenous sources. One of the most deleterious manifestation is DNA double strand breaks (DSBs), as failure to repair a DSB can lead to loss of genetic information and be an underlying cause for tumor progression in higher eukaryotes (Hanahan & Weinberg, 2011; Jackson & Bartek, 2009). Cells have two main pathways to repair DSBs. First, Homologous Recombination (HR) is carried out in the S/G2 phase of the cell cycle, relies on 5'-3' resection of the broken DNA ends and uses the homology on the sister chromatid as a template for repair (Symington, 2016). Second, Non-Homologous End Joining (NHEJ) is carried out throughout the cell cycle but it is the dominant form of repair in the G1 phase. NHEJ may or may not use processing of the broken ends before ligation, making it a more error-prone pathway than HR (Chiruvella *et al*, 2013). Cells also have backup repair pathways such as Single Strand Annealing (SSA) and alt-NHEJ, which share some components with HR and NHEJ, respectively. These pathways come into play under special conditions when the main repair pathways are hindered due to genetic mutations, absence of sister chromatid and state of the cell cycle (Bhargava *et al*, 2016; Ceccaldi *et al*, 2016).

The yeast NuA4 histone acetyltransferase complex is essential for cell viability, is composed of 13 subunits and is homologous to the mammalian TIP60/p400 complex (Auger *et al*, 2008; Doyon *et al*, 2004). NuA4/TIP60 acetylates histones H4 and H2A N-terminal tails in chromatin, as well as variants H2A.X/H2A.Z (Allard *et al*, 1999; Clarke *et al*, 1999; Keogh *et al*, 2006; Soria *et al*, 2012; Steunou *et al*, 2014). NuA4/TIP60 has been well documented for its role in transcription regulation, at the initiation and elongation steps (Doyon & Côté, 2004; Rossetto *et al*, 2014). NuA4 is also known to acetylate non-histone proteins and regulate a variety of

cellular processes such as autophagy and gluconeogenesis (Lin *et al*, 2009; Yi *et al*, 2012). Temperature sensitive mutants of Esa1, the yeast catalytic subunit, as well as point mutants of H4 and H2A target lysine residues show grown defects in presence of various DNA damaging chemical agents, underpinning the importance of NuA4 and acetylation for the repair of DNA breaks (Allard *et al.*, 1999; Auger *et al.*, 2008; Bird *et al*, 2002; Choy & Kron, 2002; Downs *et al*, 2004). NuA4 has been shown to play an important role for the recruitment of chromatin remodelers such as INO80, SWI/SNF and RSC to DNA repair sites (Bennett & Peterson, 2015; Downs *et al.*, 2004; House *et al*, 2014). Our recent work indicates that NuA4 is rapidly recruited to a DSB by the MRX complex (Mre11-Rad50-Xrs2) and this is most likely through a DNA damage-induced phospho-dependent interaction with the Xrs2 protein (Cheng *et al*, 2018). In addition, we have shown that NuA4 directly acetylates RPA to modulates its dynamic association with ssDNA during the repair process (Cheng *et al.*, 2018). NuA4 has also been implicated in opposing Rad9 checkpoint activity after DNA damage in budding yeast (Clarke *et al.*, 1999; Javaheri *et al*, 2006). This is paralleled by the mammalian TIP60 complex which was shown to antagonizes 53BP1 (homolog of yeast Rad9) in the vicinity of DSBs to favor repair by HR (Jacquet *et al*, 2016; Tang *et al*, 2013). Tip60-dependant acetylation and activation of ATM has also been argued to be involved in DNA damage signaling (Dantuma & van Attikum, 2016).

In this study we dissected the functional relationship of NuA4 with the NHEJ repair pathway. We show that, upon removal of NHEJ factors, NuA4 is strongly recruited to DSBs during the G1 phase of the cell cycle, along DNA end resection, in a Xrs2 and Lcd1/Ddc2-dependent manner. Conditions of defective NuA4 acetyltransferase activity decrease the hyper-resection phenotype, suggesting that NuA4 can play a role in a resection-based repair pathway in G1. In

addition, NHEJ core factors Nej1 and Yku80 are targets of NuA4-dependent acetylation which lowers NHEJ efficiency, disrupt physical interactions and increases resection. Our results support a model in which NuA4 favors repair of DSBs by resection-based pathways in part through inhibition of NHEJ factors.

RESULTS

Deletion of NHEJ factors leads to recruitment of NuA4 at DSBs in G1

Yeast Rad9, similar to its mammalian homolog 53BP1, is known to slow down or to keep a check on the rate of DNA end resection (Escribano-Díaz *et al*, 2013; Ferrari *et al*, 2015; Noordermeer *et al*, 2018; Zimmermann *et al*, 2013). 53BP1 has been shown to have an antagonistic relationship with mammalian NuA4/TIP60 (Tang *et al.*, 2013). They compete to bind the H4K20me mark and target H2AK15 modifications, implicating them in the selection of the DSB repair pathway (Jacquet *et al.*, 2016). In yeast, NuA4 mutant cells accumulate in the G2 phase at non-permissive temperature, in a Rad9-dependent manner (Clarke *et al.*, 1999). In addition, NuA4 mutants defective in acetylation show a strongly increased Rad9-dependent G1 checkpoint upon DNA damage, implicating NuA4 in an antagonistic relationship with Rad9 during the DNA damage response (Javaheri *et al.*, 2006).

Yeast Rad9 binds chromatin near DSBs through bivalent interaction with two histone marks, H3K79me by its Tudor domain and H2AS129ph by its BRCT domain (γH2A) (Grenon *et al*, 2007; Hammet *et al*, 2007; Wysocki *et al*, 2005)**.** To determine if Rad9 binding to chromatin can affect NuA4 activity (Fig 1A), we performed *in vitro* histone acetyltransferase (HAT) assays using native chromatin purified from cells treated with a DNA damaging agent, MMS. Wild type and

Tudor or BRCT mutant recombinant Rad9 (aa639-1308, Fig EV1A) were incubated with chromatin and purified native NuA4 complex, followed by HAT assay with radioactive Acetyl-CoA. Wild type Rad9 is able to significantly block acetylation of nucleosomes by NuA4, whereas Rad9-Y798Q and Rad9-K1088E are less efficient at doing so, reflecting their decreased ability to bind chromatin (Fig 1B).

We have recently shown that NuA4 is recruited to DSBs mainly during the S/G2 phase of the cell cycle (Cheng *et al.*, 2018). To study whether Rad9 may affect recruitment of NuA4 at DSBs *in vivo*, we deleted *RAD9* and performed chromatin immunoprecipitations (ChIP)-qPCR at the HO-induced DSB in asynchronous and G1-arrested cells. It is important to indicate all the ChIP experiments presented in this study are controlled for consistent level of HO-induced DSB formation (Fig EV1D-H) as well as tight synchronization of cells in G1 (*bar1* mutant background, FACS and microscopic analysis). While asynchronous cells show no significant difference in NuA4 binding between wild type and *RAD9* deletion mutant (Fig EV1B), G1 synchronized cells show a small but significant increase in the recruitment of NuA4 (Fig 1C), along with the expected increase of DNA end resection as measured with Rfa1, the largest subunit of RPA (Fig 1D).

Deletion of yeast Ku (Yku) in asynchronous cells do not significantly affect recruitment of NuA4 at the HO-induced DSB (Cheng *et al.*, 2018). However, cells synchronized in G1 phase show strong recruitment of NuA4 at the DSB in the absence of Yku80 (Fig 1E). ChIPs with Rfa1 also show strongly increased signal for RPA around the DSB site, indicating abnormal high DNA end resection in G1 (Fig 1F). We wanted to know if this antagonistic relationship was exclusive for Yku or extended to other NHEJ factors. Deletion of *NEJ1*, a core NHEJ factor, in G1 synchronized cells

results again in increased NuA4 recruitment around the HO DSB (Fig 1G), as well as higher resection (Fig 1H), which is not observed in asynchronous cells (Fig EV1C).

In parallel, *RAD9* was deleted in the *HDF2* (*YKU80*) deleted background. Previous studies have shown that the double deletion of *RAD9* and *HDF1* (*YKU70*) results in hyper-resection of DNA ends at DSBs in the G1 phase of the cell cycle (Trovesi *et al*, 2011). We confirmed this finding as indicated by a very strong increase of Rfa1 signal seen in *rad9*Δy*ku80*Δ cells (Fig 1F). Interestingly, a similar effect is observed for NuA4, with the double deletion mutant giving a much stronger signal compared to single y*ku80*Δ cells (Fig 1E). Altogether, these data demonstrate that the NuA4 complex can be efficiently recruited at a DSB in G1 in the absence of core NHEJ factors, Yku80 and Nej1, and also with the deletion of *RAD9*. This supports the concept of an antagonistic relationship between NuA4 and the NHEJ machinery for repair of DNA breaks.

Xrs2-dependent recruitment of NuA4 at DSB in G1

NuA4 subunit Tra1 shows high domain homology with Tel1/ Mec1, members of the PIKK family. Both Tel1 and Mec1, like their mammalian counterpart ataxia telangiectasia mutated (ATM), AT-related (ATR) and DNA-dependent protein kinase (DNA-PK), are important for signaling of the DSB and recruitment of downstream repair proteins (Abraham, 2001; Smith & Jackson, 1999). We have recently shown that Tra1 gets phosphorylated upon DNA damage and its C-terminus containing the PI3K-like domain can directly bind Xrs2 *in vitro*, an interaction likely involved in the recruitment of NuA4 at the HO induced DSB site (Cheng *et al.*, 2018). To understand if Xrs2 is required for NuA4 recruitment at the DSB in G1, we performed ChIP-qPCR in *XRS2* deletion background. As seen in (Fig 2A), the NuA4 signal detected in G1 in the absence of Rad9 is

completely lost when *XRS2* is deleted. The same can be said for end resection measured Rfa1/RPA (Fig 2B). Strikingly, deletion of *XRS2* in the background with hyper-resection (*rad9*Δy*ku80*Δ) also abrogates NuA4 recruitment and resection in G1 cells (Fig 2C-D). Since deletion of *XRS2* blocks resection, it was unclear whether the loss of NuA4 recruitment is directly due to the loss of interaction with Xrs2 or to the loss of resection itself. The *mre11-H125N* nuclease-defective mutant background was used to address this issue since it is known to slow down rate of resection in G1 synchronized cells (Clerici *et al*, 2008). As seen in (Fig 2E-F), while there is a decrease in the Rfa1 signal close to the break, NuA4 detection seems unaffected. These results indicate that NuA4 recruitment at a DSB in G1 requires the Xrs2 subunit of the Mre11/Rad50/Xrs2 (MRX) complex.

Lcd1/Ddc2-dependent recruitment of NuA4 at DSBs

Xrs2 harbors the Nuclear Localization Sequence (NLS) required for Mre11 import into the nucleus. Thus, loss of Xrs2 results in failed assembly of the MRX complex (Tsukamoto *et al*, 2005). To overcome this issue, we used a low copy number plasmid expressing Mre11 fused to a NLS (referred to as *MRE11-NLS*). In accordance with previous studies, expression of Mre11-NLS suppresses the growth defect of *xrs2*Δ cells in the presence of a DNA damaging agent (MMS, Fig EV3A) (Oh *et al*, 2016; Tsukamoto *et al.*, 2005). Interestingly, expression of Mre11-NLS in G1 cells carrying the double deletion *rad9*Δy*ku80*Δ in addition to *xrs2*Δ leads to a significant increase in NuA4 recruitment and resection (Fig 3A-B). This result demonstrates an Xrs2-independent mode of NuA4 recruitment at DSBs. Importantly, this Xrs2-independent mechanism is not restricted to

cells in G1 as asynchronous cells also show a rescue for NuA4 recruitment and resection with the introduction of *MRE11-NLS* in *xrs2*Δ cells (Fig 3C-D).

We previously reported that the Tra1 subunit of NuA4 can interact directly with Lcd1 (ATRIP in mammals) *in vitro* (Cheng *et al.*, 2018). Lcd1/Ddc2 is the binding partner of Mec1 (ATR in mammals) and is responsible for the recruitment of Mec1 onto the RPA-coated ssDNA generated by resection (Zou & Elledge, 2003). To establish whether NuA4 interaction with Lcd1/Ddc2 is the alternate mechanism of NuA4 recruitment seen above in the absence of Xrs2, we deleted *LCD1* (in a *SML1* deleted background to overcome the synthetic lethality) (Gobbini *et al*, 2013; Paciotti *et al*, 2000). However, the introduction of *MRE11-NLS* in this background is insufficient to rescue resection, making conclusions about NuA4 recruitment difficult (Fig EV3D-E). To overcome this issue, we overexpressed long range resection exonuclease Exo1. Expression of Mre11-NLS along with Exo1 overexpression leads to a diminished DNA signal after DSB induction, indicating DNA end resection (Fig 3E)**.** This is dependent on Exo1 activity since a nuclease dead mutant of the protein (Exo1-D173A) behaves like the empty vector control (EV). However, in these mutant conditions allowing some DNA end resection, NuA4 signals around the DSB do not change significantly in the absence of Lcd1 and Xrs2 (Fig 3F). Therefore, these results support the idea that the Xrs2-independent mode of NuA4 recruitment at DSBs is through interaction with Lcd1/Ddc2.

NuA4-dependent acetylation is important for hyper-resection in G1 cells

DSBs flanked by direct repeats are repaired by a Rad52-dependent pathway called single strand annealing (SSA). The resected ends anneal at the repeats and the intervening DNA along with one

repeat are removed by a nucleolytic process (Ivanov *et al*, 1996). It has been well documented that Rad52 is essential for repair of DSBs by SSA in G1 cells (Trovesi *et al.*, 2011). To investigate NuA4 possible function in such process, we performed ChIP-qPCR to measure Rad52 recruitment to DSBs in G1 and our mutant backgrounds. As expected in the hyper-resection *rad9*Δy*ku80*Δ mutant background, very high recruitment of Rad52 is detected in G1 cells (Fig 4A). This is also seen in the *nej1*Δ background, albeit to a lower level similar to the y*ku80*Δ single mutant (Fig 4A-B). Similar to a previous study (Zhang *et al*, 2007), we also observed recruitment of Rad51 in y*ku80*Δ and *rad9*Δy*ku80*Δ G1-blocked cells (Fig EV4A).

To determine whether NuA4 has a role in this G1 phase mechanism of DSB repair, we introduced the *esa1-L254P* temperature sensitive (ts) mutant allele which affects the acetylation capacity of NuA4 even at semi-restrictive temperature (as shown by western blot for the H4ac in Fig 4C**)**(Clarke *et al.*, 1999). Interestingly, Rfa1 ChIP-qPCR to measure the hyper-resection phenotype in the triple *rad9*Δy*ku80*Δ*esa1-ts* triple mutant background shows a significant reduction of DNA end resection compared to the *rad9*Δy*ku80*Δ double mutant (Fig 4D). These results indicate that NuA4 acetyltransferase activity is important to stimulate DNA end resection in G1, likely in part through acetylation of chromatin in front of the resection machinery. This is supported by a partial suppression of the DNA damage sensitivity of *esa1-ts* mutant cells by the *rad9*Δy*ku80*Δ deletions (Fig 4E). On the other hand, we cannot observe a clear effect of NuA4 partial loss of function on Rad52 recruitment in these conditions in G1 cells (Fig EV4B).

Acetylation of Nej1 by NuA4 in the regulation of DSB repair pathway choice

Yeast Nej1 and its mammalian homologs XLF/NHEJ1 and PAXX have been shown to be important for repair by NHEJ (Chang *et al*, 2017; Kegel *et al*, 2001; Ooi *et al*, 2001; Valencia *et al*, 2001). Nej1 acts as a scaffolding protein for other NHEJ factors, the N-terminal of Nej1 interacting with Yku and its C-terminal with Lif1 (Deshpande & Wilson, 2007; Mahaney *et al*, 2014; Sulek *et al*, 2007). XLF has also been shown to interact with mammalian Ku and XRCC4 (Deshpande & Wilson, 2007). Both Nej1 and Dnl4-Lif1 are required for retention/stabilization of Yku at DSBs (Chen & Tomkinson, 2011; Zhang *et al.*, 2007). Nej1, like its mammalian homolog, is important for tethering the two broken ends of the DNA (Graham *et al*, 2018; Reid *et al*, 2015) and it was also recently shown to interact with Mre11 of the MRX complex for its tethering activity (Mojumdar *et al*, 2019).

In a large-scale proteomic study, Nej1 was shown to be a target of NuA4 acetyltransferase activity *in vitro* (Lin *et al.*, 2009). To investigate this further and its *in vivo* relevance, we purified Nej1 from yeast cells and compared the acetylated lysines detected by mass spectrometry from wild type and the *esa1-L254P* NuA4 mutant backgrounds. Three lysine residues, K18, K192 and K234, were detected to be acetylated on Nej1 in WT conditions but not in the mutant background (Fig EV5A). To determine if these acetylation sites are important for Nej1 function, we produced yeast strains that express Nej1 with non-acetylatable (K to R) or acetylation-mimic (K to Q) substitutions. Importantly, the point mutations do not affect the stability of Nej1 (Fig 5A). Next, we tested if these lysines affect the efficiency of DSB repair by NHEJ. As shown in (Fig 5B), loss of Nej1 completely abrogates repair by NHEJ, measured by re-ligation efficiency for digested plasmid templates. Interestingly, both acetyl (3KQ) as well as non-acetyl (3KR) substitution mutants show significantly decreased NHEJ efficiency. These results demonstrate the importance

of these three lysine residues in Nej1 function during DSB repair by NHEJ. In contrast, Nej1 wild type and mutants show similar repair efficiency for a chromosomal DSB at the *MAT* locus (Fig EV5B). Importantly, ChIP-qPCRs for NuA4 and RPA around the HO-induced DSB in G1 cells show significantly increased recruitment of NuA4 as well as resection in the acetyl mimicking *nej1* mutant (Fig 5C-D; the non-acetyl *nej1* mutant datapoints overlap with the wild type ones). The increases seen in the *nej1-3KQ* background do not reach the levels obtained with the complete loss of Nej1. This could be due to Nej1-3KQ still getting recruited at the break, but with impaired function. Since Nej1 interaction with other NHEJ factors is important for its function (Chen & Tomkinson, 2011; Mahaney *et al.*, 2014; Mojumdar *et al.*, 2019; Sorenson *et al*, 2017; Sulek *et al.*, 2007), we performed *in vitro* protein-protein interaction analysis using Nej1 mutants with Yku80 and Lif1. While wild-type Nej1 and the 3KR mutant show similar interaction with Yku80, the acetyl mimicking 3KQ mutant shows less binding (Fig 5E). In parallel, interaction of Nej1 with Lif1 is significantly decreased in both 3KQ and 3KR mutants compared to wild type (Fig 5F). The decreased binding of Nej1-3KR with Lif1 but not with Yku80 could explain its effect on the plasmid re-ligation assay (Fig 5B). Lif1 binds the Dnl4 ligase and loss of a stable interaction with Nej1 may result in defective Lif1-Dnl4 recruitment, leading to impaired DSB religation. However, since Nej1-3KR is still able to interact with Yku80, stabilizing it at the break, it can explain the absence of effect on resection compared to wild type cells (Fig 5D). Furthermore, the Nej1-3KQ acetyl-mimic mutant also shows decreased binding to the C-terminal part of Mre11 compared to wild type and the 3KR mutant, which may affect its tethering activity (Fig EV5D). Importantly, Nej1 phosphorylation in response to DNA damaging agents (Ahnesorg & Jackson, 2007) is not affected by the 3 lysine substitutions or the depletion of NuA4 acetyltransferase activity (Esa1) using the

anchor-away system (Haruki *et al*, 2008; Kollenstart *et al*, 2019)(cells are treated with DNA damaging agent MMS, phosphorylation leading to the appearance of a slower migrating Nej1 signal) (Fig EV5E-G).

In mammals, NHEJ core factor Ku70 is known to get acetylated by CBP which inhibits DNA repair and regulates Bax-mediated cell apoptosis (Cohen *et al*, 2004; Li *et al*, 2020). We tested if yeast Ku is also acetylated in yeast cells and if it could be a non-histone target of NuA4, along with Nej1. Using the anchor-away system to deplete Esa1 (Fig EV5G) and immunoprecipitation with an anti-acetyl-lysine antibody, we demonstrate that Yku80 is indeed acetylated *in vivo* and NuA4 is clearly required for most of this acetylation to occur (Fig 5G). Interestingly, Yku80 acetylation seems slightly higher in conditions of DNA damage. Taken together, these data indicate that Nej1 and Yku80 are non-histone substrates of NuA4 acetyltransferase activity. Acetylation of Nej1 may reduce NHEJ efficiency by disrupting its interaction with Yku80 and Lif1. Further studies are required to characterize the effect of acetylation on Yku80 function but work in higher eukaryotes also supports an inhibitory role.

DISCUSSION

Altogether, the results of this study allow us to untangle two modes of recruitment for NuA4 at DSBs. The Xrs2-dependent pathway is responsible for initial recruitment of NuA4 (Fig 2), as we previously reported (Cheng *et al.*, 2018). This happens early during DSB signaling and the repair process when MRX is recruited to the break site. It is known that PIKK family member Tra1, subunit of NuA4, can directly interact with Xrs2 (Cheng *et al.*, 2018). The other main acetyltransferase complex in yeast, SAGA, also contains Tra1 and requires Xrs2 for its recruitment

at the break (Cheng *et al.* unpublished). Tra1 is therefore related to the Tel1(ATM) signaling kinase not only at the amino acid sequence but also in its mode of recruitment at the DNA break being dependent on Xrs2 (Oh *et al.*, 2016). Tel1 signals the DSB by phosphorylation of H2A-S129 (γ-H2A) in the surrounding chromatin (Harrison & Haber, 2006). The nucleolytic processing, termed resection of the DNA breaks produces 3' ssDNA ends. This ssDNA gets coated by RPA to prevent secondary structure formation and degradation. RPA-coated ssDNA is recognized by various repair proteins, one such being Lcd1/Ddc2(ATRIP) (Symington, 2016; Zou & Elledge, 2003). We had shown previously that Tra1 can also directly interact with Lcd1 *in vitro (Cheng et al., 2018)*. Our *in vivo* data support this link as NuA4 can be detected at the break in the absence of Xrs2 and this is dependent on Lcd1 (Fig 3C, F and EV3E).

Resection is the event that marks the commitment of DSB repair to the HR process. The 3' ended ssDNA searches for the homologous sequence or sister chromatid to use as a template to complete the repair process (Symington, 2016). Resection is a very regulated process and is active in S/G2 phase when the Cdk1 activity is high and inhibited during the G1 phase of the cell cycle when Cdk1 activity is low (Trovesi *et al.*, 2011). But it has been shown previously that resection can be achieved in G1 phase with the deletion of Ku protein (Trovesi *et al.*, 2011; Zhang *et al.*, 2007). In mammalian cells, HR in G1 phase requires deletion of the *RAD9* homolog 53BP1, depletion of KEAP1 and a phospho-mimicking mutant of CtIP (Orthwein *et al*, 2015). In our experiments we detect efficient NuA4 recruitment at a DSB in G1 concomitant with the appearance of resection (Fig 1). It was previously shown that deletion of NHEJ factors in G1 not only leads to resection but also repair of the DSB by SSA, relying on the recombination protein Rad52 (Trovesi *et al.*, 2011). Our question then was to evaluate if NuA4 played a role in this

resection-based repair in G1. Temperature sensitive mutant of Esa1, the catalytic subunit of NuA4, slows down resection which likely impairs such repair process requiring extended end resection (Fig 4D). This implicates NuA4 as one of the key players in the resection-based G1 repair pathways. NuA4-dependent acetylation of histone H4 and H2A tails has been shown to be important for recruitment of various chromatin remodelers (INO80, SWI/SNF, RSC) and required for fidelity of HR repair process (Bennett & Peterson, 2015; Downs *et al.*, 2004; House *et al.*, 2014). It will be interesting to verify if remodelers are also important and regulated by NuA4 during repair in G1.

We were able to demonstrate that two NHEJ core factors, Nej1 and Yku80, are new non-histone targets of NuA4 acetyltransferase activity (Fig EV5A, 5G). Nej1 has previous been reported to be critical for NHEJ repair (Kegel *et al.*, 2001; Ooi *et al.*, 2001; Valencia *et al.*, 2001) and our *nej1* acetyl mutants also show impaired NHEJ (Fig 5B). Nej1 is known to act as a scaffold for binding and stabilizing other proteins of the NHEJ machinery (Chen & Tomkinson, 2011; Deshpande & Wilson, 2007; Mahaney *et al.*, 2014; Sulek *et al.*, 2007). Nej1 acetyl-mimicking mutant shows reduced binding to Lif1 and Yku80 *in vitro*, which correlates with increased resection seen *in vivo* (Fig 5D-F). It would be interesting to determine how these individual lysines affect interaction of Nej1 with other NHEJ proteins and whether the tethering activity of Nej1 itself is impaired in these mutants (Mojumdar *et al.*, 2019). In both yeast and mammals, it has been documented that Ku may interact with various histone deacetylases (HDACs) and these have an important role in repair by NHEJ (Boulton & Jackson, 1998; Jeong *et al*, 2007; Miller *et al*, 2010). Further analysis of NuA4 interplay with NHEJ would include identification of the specific lysines on Yku80 that get acetylated by NuA4. Removal of positive charge of lysines through

acetylation may reduce or abrogate the binding capacity of Yku80 to DNA at the break site leading to processing/ resection of the DNA ends. The acetylation may also affect the binding with Yku70 and formation of the Ku complex, there by impairing NHEJ.

Our data supports a model (Fig 6) in which NuA4 is recruited by the MRX complex in the early steps after DSB formation. Since Rad9 and other NHEJ factors get assembled at the break, these, apart from inhibiting resection, may also inhibit acetylation of chromatin by NuA4. If NuA4 is able to directly acetylate Nej1, this blocks the assembly of the NHEJ repair machinery, thereby favoring the initiation of DNA end resection. Resection then leads to RPA-coated ssDNA, recruitment of Lcd1/ATRIP and subsequent NuA4 spreading away from the break, helping long-range resection in the context of chromatin. Our results clearly demonstrate that NuA4 regulates the repair pathway choice, away from NHEJ, and favors repair by resection-based processes throughout the cell cycle. It supports and greatly broadens the conclusions of our previous work that highlighted a crucial battle between 53BP1 and NuA4/TIP60 to regulate DSB repair pathway choice. Future work will verify if the mammalian NuA4/ TIP60 complex also targets NHEJ proteins during regulation of repair pathway choice. It is also possible that NuA4 is involved in other DSB repair pathways such as alt-NHEJ, underpinning its role in resection-based repair. A better understanding of how NuA4/TIP60 gets recruited to the DNA damage site and acetylates specific non-histone proteins to modulate repair, identifies new molecular targets that can be acted upon to treat diseases such as cancer.

MATERIAL AND METHODS

Yeast strains and growth assay

Yeast strains used in the current study are listed in appendix table S1. Standard PCR based protocol was used for respective transformations employing the lithium acetate method. Yeast cells were grown in YPD (1% yeast extract, 2% peptone, 2% dextrose) at 30°C or in synthetic complete media. For DSB induction, cells were grown at 30 ^{o}C overnight in YP-Raffinose and 2% galactose was added for 3 hours to induce HO endonuclease.

Yeast spot assays were performed with yeast culture grown overnight in YPD at 23°C and SC-URA at 30°C, inoculated in the morning in YPD/ SC-URA at OD_{600} 0.3 and grown for 3–4 hours. The 10-fold serial dilutions of the yeast cultures were made for spotting on YPD/ SC-URA plates supplemented with methylmethane sulfonate (MMS). Colonies were allowed to grow for 3-4 days at 32°C for YPD and 30°C for SC-URA plates and the growth sensitivities were compared to YPD/ SC-URA control plate.

Chromatin Immunoprecipitation (ChIP)

ChIP-qPCR was performed as described previously (Rossetto *et al.*, 2014). In short, yeast cells were grown in YP-Raff till optical density (O.D. 600) of the culture was between ~0.5 to 1. α-factor was added to the indicated experiments for 6 hours to synchronize the cells in G1 phase. This was followed by addition to galactose for 3 hours to induce DSB at MAT locus. Next, cells were cross-linked with formaldehyde and cells were lysed by bead beating. Sonication was performed (Diagenode Bioruptor) to obtain chromatin size of ~200-500 bp. 100ug of chromatin was incubated with the indicated antibody overnight on a wheel at 4°C. Next day, protein A or G sephrose beads were added followed by subsequent washing steps and overnight at 65°C for de-

cross linking. Phenol chloroform extraction was performed, and DNA samples were dissolved in NTE to be used for qPCR. LC480 LightCycler (Roche) was used to quantify DNA with the primer pairs flanking the indicated region left (0.15bp, 1Kb, 3Kb, 7Kb) and right (1kb, 3Kb, 7Kb) of induced DSB at MAT locus. Homothallic endonuclease (HO) cutting efficiency at MAT locus was calculated using qPCR with primer pair spanning the HO cut site normalized to uncut control site, interV (long intergenic region on chromosome V). Primer sequences are available upon request. Antibodies used for ChIP are as follows: anti-Eaf1 (Auger *et al.*, 2008), anti-Rfa1 (Agrisera AS 07214), anti-Rad51(Santa Cruz y-180), anti-Rad52(Santa Cruz yC-17).

Recombinant protein purification and pull-down assay

Recombinant proteins were purified from BL-21 bacteria using standard protocol described previously (Setiaputra *et al*, 2018). In brief, bacterial culture was growth overnight at 16°C in presence of IPTG. Bacterial pellet was treated with lysozyme and sonicated. Soluble fraction was incubated with Ni-nitrilotriacetic acid (NTA)-agarose (Qiagen) beads or glutathione-sepharose (GE Healthcare) for 3-4 hours on wheel at 4°C for His- or GST-tagged proteins respectively. Coomassie blue staining was performed to estimate purified protein concentration with known bovine serum albumin (BSA) standards. After elution ~300-600 ng of His-tagged protein were pre-cleared with glutathione sepharose beads and incubated with immobilized GST-tagged protein in binding buffer (25 mM HEPES [pH 7.5], 100 mM NaCl, 10% glycerol, 100 μg/ml BSA, 1 mM PMSF, 0.5 mM dithiothreitol [DTT], 0.1% Tween 20, and protease inhibitors) at 4°C for 3 hours followed by washing the beads three times. 1 μg of GST only immobilized protein was used as control. After washing Laemmli buffer 1X was added followed by boiling and loading on SDS-

PAGE for visualization by western blotting using anti-His (Clonetech 631212) and anti-GST (Sigma G1160) antibodies.

Purification of acetylated Nej1 for mass spectrometry

GST-tagged Nej1 was purified from wild-type and *esa1-L254P* (ts) background, followed by mass spectrometry analysis to identify the acetylation sites as described previously with few modifications (Lin *et al.*, 2009). In short, cells were grown in SC-Ura containing 2% raffinose till OD_{600} ~0.8-1.0. Galactose (2% final) was added for the induction of the GST-tagged Nej1 and cells were grown at 37°C for two additional hours. Cells were harvested and lysed in extraction buffer (10mM Tris-HCl pH 8.0, 350mM NaCl, 0.1% NP-40, 10% glycerol, 1mM DTT, 1mM PMSF, 2 µg/mL leupeptin, 2 µg/mL pepstatin A, 5 µg/mL aprotinin, 5 mM β-glycerophosphate, 10 mM sodium butyrate, 5 mM NaF, 10mM nicotinamide, 15µM TSA). The lysate was centrifuged at 10,000g for 30min at 4°C, followed by ultracentrifugation for 1 hour at 45,000g. The supernatant was precleared with CL6B beads (Sigma) before the addition of glutathione-sepharose beads (GE Healthcare) for 3 hours on wheel at 4°C. After binding the glutathione-sepharose beads were washed 5 times with wash buffer (20mM Hepes pH7.5, 200mM NaCl, 10mM sodium butyrate). Beads were mixed with elution buffer (50mM Tris-HCl pH8.0, 10mM glutathione, 10% glycerol, 5mM sodium butyrate) at 4°C on wheel and first elution was collected after 1 hour and other after overnight incubation. Next, protein A-sepharose beads were washed with IP lysis buffer (75mM Tris-HCl ph 7.5, 50mM NaCl, 1mM EDTA, 1mM EGTA, 10% glycerol, 1% Tween-20, 1mM DTT, 1mM PMSF, 5mM NaF, 2 µg/mL leupeptin, 2 µg/mL pepstatin A, 5 µg/mL aprotinin, 10mM sodium butyrate, 10mM, nicotinamide, 15µM TSA, 1 µM MG132) and conjugated with 6µl of mouse monoclonal anti-acetylated-lysine (Cell Signalling 9681S). Antibody conjugated protein A-

sepharose beads were incubated with GST elution at 4°C for 3 hours on a wheel. After washing 4 times with IP wash buffer (50mM Hepes pH 7.0, 100mM NaCl, 10 mM sodium butyrate) 20 µl of SDS-PAGE sample buffer was added and boiled. The samples were resolved by SDS-PAGE followed by colloidal Coomassie blue staining to visualize and cut gel bands, which were send for mass spectrometry analysis after trypsin digestion.

Chromatin binding and histone acetyltransferase assay

Histone acetyltransferase assay was performed as described (Allard *et al.*, 1999; Steunou *et al*, 2016). 500ng of short oligonucleosomes purified from methyl methanesulfonate MMS (0.05%) treated yeast cells, was incubated with recombinant Rad9 at 30°C for 30 min. This was followed by the addition of NuA4 complex and 0.125 µCi of [^{3}H]acetyl coenzyme A ([3H]acetyl-CoA) in HAT buffer (50 mM Tris-HCl [pH 8], 50 mM KCl plus NaCl, 0.1 mM EDTA, 5% glycerol, 1 mM DTT, 1 mM PMSF and 20 mM sodium butyrate) at 30°C for 30 min. The reaction mixture was spotted on p81 filter paper, washed and air dried. The incorporation of radiolabeled acetylation was measured by scintillation counting.

Non-homologous end joining (NHEJ) assay

Plasmid re-ligation assay was performed as described (Ooi *et al.*, 2001). 0.4 µg plasmid pSO98 supercoiled or EcoR1 digested was used to transform *nej1*Δ yeast strains that harbored wild type or mutant form of the *NEJ1* gene on a CEN:ARS low copy number plasmid. The transformed yeast was plated on SC-His-Leu and SC-His-Ura and kept at 30°C. After 3 days colonies were counted and ratio of colonies transformed with digested plasmid to undigested supercoiled plasmid was taken. Data represents two independent biological replicates and error bar denotes the range between the biological replicates.

Chromosomal NHEJ assay was performed as described (Valencia *et al.*, 2001). Yeast background used carries deletion of *HML* and *HMR* and galactose-inducible HO endonuclease that creates a single DSB at the *MAT* locus. Endogenous *NEJ1* gene was deleted and wild type or mutant form of the *NEJ1* gene was expressed from a low copy number CEN:ARS plasmid. The yeast cells were grown overnight in YP-Raffinose media. Next day appropriate number of cells in the log phase were plated on YP-Galactose and YP-Glucose plates and kept at 30°C. After 3-4 days the number of colonies was quantified and ratio of colonies on YP-Galactose to YP-Glucose was calculated. Data are from three independent biological replicates and error bar denotes the standard deviation between the replicates.

Acetyl-lysine Immunoprecipitation

Immunoprecipitation was performed as described previously (Cheng *et al.*, 2018). Cells were grown in YPD till OD600 was ~0.5 followed by rapamycin addition (1μg/ml final) for 30 mins. MMS (0.05%) or DMSO was added for 2 hours. Cells were collected and lysed in 10 mM Tris-HCl pH 8.0, 150 mM NaCl, 10% glycerol, 0.1% NP-40, 2 μg/mL leupeptin, 2 μg/mL pepstatin A, 5 μg/mL aprotinin, 1 mM PMSF, 10 mM β-glycerophosphate, 1 mM Sodium Butyrate, 0.5 mM NaF, and 1 mM DTT. 4 μg of WCE was incubated with anti-acetyl (ImmuneChem ICP0380), overnight at 4°C. Protein G Dynabeads (Invitrogen 10004D) was added to the reaction and kept on wheel at 4°C for 4 additional hours. The IPs were washed and 1X Laemmli buffer was added and boiled. The samples were resolved on SDS-PAGE followed by western blotting and analyzed with anti-Myc (9E10 Babco MMS150R) and anti-Pgk1 (Abcam 113687).

Acknowledgments

We thank Olivier Jobin-Robitaille pour early work on this project, Zhiyou Deng and Yingming Zhao (U. of Chicago) for mass spectrometry analysis of Nej1. We thank James E. Haber and Jennifer Cobbs for stimulating discussions. We are grateful to Lorraine S. Symington for providing plasmids. This work was supported by a grant from the Canadian Institutes of Health Research (CIHR) to J.C. (FDN-143314). S.A. held a Desjardins/Fondation du CHU de Québec studentship and X.C. a FRQS studentship. J.C. holds the Canada Research Chair in Chromatin Biology and Molecular Epigenetics.

Author contributions

SA, VC, XC, GB and MA performed experiments. SA and JC designed experiments, analyzed the data and prepared the manuscript.

Conflict of interest

The authors declare that they have no conflict of interest.

REFERENCES:

Abraham RT (2001) Cell cycle checkpoint signaling through the ATM and ATR kinases. *Genes & Development* 15: 2177-2196

Ahnesorg P, Jackson SP (2007) The non-homologous end-joining protein Nej1p is a target of the DNA damage checkpoint. *DNA Repair* 6: 190-201

Allard S, Utley RT, Savard J, Clarke A, Grant P, Brandl CJ, Pillus L, Workman JL, Côté J (1999) NuA4, an essential transcription adaptor/histone H4 acetyltransferase complex containing Esa1p and the ATM-related cofactor Tra1p. *The EMBO Journal* 18: 5108-5119

Auger A, Galarneau L, Altaf M, Nourani A, Doyon Y, Utley RT, Cronier D, Allard S, Côté J (2008) Eaf1 Is the Platform for NuA4 Molecular Assembly That Evolutionarily Links Chromatin Acetylation to ATP-Dependent Exchange of Histone H2A Variants. *Molecular and Cellular Biology* 28: 2257-2270

Bennett G, Peterson CL (2015) SWI/SNF recruitment to a DNA double-strand break by the NuA4 and Gcn5 histone acetyltransferases. *DNA Repair* 30: 38-45

Bhargava R, Onyango DO, Stark JM (2016) Regulation of Single-Strand Annealing and its Role in Genome Maintenance. *Trends in genetics : TIG* 32: 566-575

Bird AW, Yu DY, Pray-Grant MG, Qiu Q, Harmon KE, Megee PC, Grant PA, Smith MM, Christman MF (2002) Acetylation of histone H4 by Esa1 is required for DNA double-strand break repair. *Nature* 419: 411-415

Boulton SJ, Jackson SP (1998) Components of the Ku-dependent non-homologous end-joining pathway are involved in telomeric length maintenance and telomeric silencing. *The EMBO Journal* 17: 1819-1828

Ceccaldi R, Rondinelli B, D'Andrea AD (2016) Repair Pathway Choices and Consequences at the Double-Strand Break. *Trends in cell biology* 26: 52-64

Chang HHY, Pannunzio NR, Adachi N, Lieber MR (2017) Non-homologous DNA end joining and alternative pathways to double-strand break repair. *Nature Reviews Molecular Cell Biology* 18: 495-506

Chen X, Tomkinson AE (2011) Yeast Nej1 Is a Key Participant in the Initial End Binding and Final Ligation Steps of Nonhomologous End Joining. *Journal of Biological Chemistry* 286: 4931-4940

Cheng X, Jobin-Robitaille O, Billon P, Buisson R, Niu H, Lacoste N, Abshiru N, Côté V, Thibault P, Kron SJ *et al* (2018) Phospho-dependent recruitment of the yeast NuA4 acetyltransferase complex by MRX at DNA breaks regulates RPA dynamics during resection. *Proceedings of the National Academy of Sciences* 115: 10028-10033

Chiruvella KK, Liang Z, Wilson TE (2013) Repair of Double-Strand Breaks by End Joining. *Cold Spring Harbor Perspectives in Biology* 5

Choy JS, Kron SJ (2002) NuA4 Subunit Yng2 Function in Intra-S-Phase DNA Damage Response. *Molecular and Cellular Biology* 22: 8215-8225

Clarke AS, Lowell JE, Jacobson SJ, Pillus L (1999) Esa1p Is an Essential Histone Acetyltransferase Required for Cell Cycle Progression. *Molecular and Cellular Biology* 19: 2515-2526

Clerici M, Mantiero D, Guerini I, Lucchini G, Longhese MP (2008) The Yku70–Yku80 complex contributes to regulate double-strand break processing and checkpoint activation during the cell cycle. *EMBO reports* 9: 810-818

Cohen HY, Lavu S, Bitterman KJ, Hekking B, Imahiyerobo TA, Miller C, Frye R, Ploegh H, Kessler BM, Sinclair DA (2004) Acetylation of the C Terminus of Ku70 by CBP and PCAF Controls Bax-Mediated Apoptosis. *Molecular Cell* 13: 627-638

Dantuma NP, van Attikum H (2016) Spatiotemporal regulation of posttranslational modifications in the DNA damage response. *The EMBO Journal* 35: 6-23

Deshpande RA, Wilson TE (2007) Modes of interaction among yeast Nej1, Lif1 and Dnl4 proteins and comparison to human XLF, XRCC4 and Lig4. *DNA repair* 6: 1507-1516

Downs JA, Allard S, Jobin-Robitaille O, Javaheri A, Auger A, Bouchard N, Kron SJ, Jackson SP, Côté J (2004) Binding of Chromatin-Modifying Activities to Phosphorylated Histone H2A at DNA Damage Sites. *Molecular Cell* 16: 979-990

Doyon Y, Côté J (2004) The highly conserved and multifunctional NuA4 HAT complex. *Current Opinion in Genetics & Development* 14: 147-154

Doyon Y, Selleck W, Lane WS, Tan S, Côté J (2004) Structural and Functional Conservation of the NuA4 Histone Acetyltransferase Complex from Yeast to Humans. *Molecular and Cellular Biology* 24: 1884-1896

Escribano-Díaz C, Orthwein A, Fradet-Turcotte A, Xing M, Young Jordan TF, Tkáč J, Cook Michael A, Rosebrock Adam P, Munro M, Canny Marella D *et al* (2013) A Cell Cycle-Dependent Regulatory Circuit Composed of 53BP1-RIF1 and BRCA1-CtIP Controls DNA Repair Pathway Choice. *Molecular Cell* 49: 872-883

Ferrari M, Dibitetto D, De Gregorio G, Eapen VV, Rawal CC, Lazzaro F, Tsabar M, Marini F, Haber JE, Pellicioli A (2015) Functional Interplay between the 53BP1-Ortholog Rad9 and the Mre11 Complex Regulates Resection, End-Tethering and Repair of a Double-Strand Break. *PLOS Genetics* 11: e1004928

Gobbini E, Cesena D, Galbiati A, Lockhart A, Longhese MP (2013) Interplays between ATM/Tel1 and ATR/Mec1 in sensing and signaling DNA double-strand breaks. *DNA Repair* 12: 791-799

Graham TGW, Carney SM, Walter JC, Loparo JJ (2018) A single XLF dimer bridges DNA ends during nonhomologous end joining. *Nature Structural & Molecular Biology* 25: 877-884

Grenon M, Costelloe T, Jimeno S, O'Shaughnessy A, FitzGerald J, Zgheib O, Degerth L, Lowndes NF (2007) Docking onto chromatin via the Saccharomyces cerevisiae Rad9 Tudor domain. *Yeast* 24: 105-119

Hammet A, Magill C, Heierhorst J, Jackson SP (2007) Rad9 BRCT domain interaction with phosphorylated H2AX regulates the G1 checkpoint in budding yeast. *EMBO reports* 8: 851-857

Hanahan D, Weinberg Robert A (2011) Hallmarks of Cancer: The Next Generation. *Cell* 144: 646-674

Harrison JC, Haber JE (2006) Surviving the Breakup: The DNA Damage Checkpoint. *Annual Review of Genetics* 40: 209-235

Haruki H, Nishikawa J, Laemmli UK (2008) The Anchor-Away Technique: Rapid, Conditional Establishment of Yeast Mutant Phenotypes. *Molecular Cell* 31: 925-932

House Nealia CM, Yang Jiahui H, Walsh Stephen C, Moy Jonathan M, Freudenreich Catherine H (2014) NuA4 Initiates Dynamic Histone H4 Acetylation to Promote High-Fidelity Sister Chromatid Recombination at Postreplication Gaps. *Molecular Cell* 55: 818-828

Ivanov EL, Sugawara N, Fishman-Lobell J, Haber JE (1996) Genetic Requirements for the Single-Strand Annealing Pathway of Double-Strand Break Repair in Saccharomyces cerevisiae. *Genetics* 142: 693-704

Jackson SP, Bartek J (2009) The DNA-damage response in human biology and disease. *Nature* 461: 1071-1078

Jacquet K, Fradet-Turcotte A, Avvakumov N, Lambert J-P, Roques C, Pandita Raj K, Paquet E, Herst P, Gingras A-C, Pandita Tej K *et al* (2016) The TIP60 Complex Regulates Bivalent Chromatin Recognition by 53BP1 through Direct H4K20me Binding and H2AK15 Acetylation. *Molecular Cell* 62: 409-421

Javaheri A, Wysocki R, Jobin-Robitaille O, Altaf M, Côté J, Kron SJ (2006) Yeast G1 DNA damage checkpoint regulation by H2A phosphorylation is independent of chromatin remodeling. *Proceedings of the National Academy of Sciences* 103: 13771-13776

Jeong J, Juhn K, Lee H, Kim S-H, Min B-H, Lee K-M, Cho M-H, Park G-H, Lee K-H (2007) SIRT1 promotes DNA repair activity and deacetylation of Ku70. *Experimental & Molecular Medicine* 39: 8-13

Kegel A, Sjöstrand JOO, Åström SU (2001) Nej1p, a cell type-specific regulator of nonhomologous end joining in yeast. *Current Biology* 11: 1611-1617

Keogh M-C, Mennella TA, Sawa C, Berthelet S, Krogan NJ, Wolek A, Podolny V, Carpenter LR, Greenblatt JF, Baetz K *et al* (2006) The Saccharomyces cerevisiae histone H2A variant Htz1 is acetylated by NuA4. *Genes & Development* 20: 660-665

Kollenstart L, de Groot AJL, Janssen GMC, Cheng X, Vreeken K, Martino F, Côté J, van Veelen PA, van Attikum H (2019) Gcn5 and Esa1 function as histone crotonyltransferases to regulate crotonylation-dependent transcription. *Journal of Biological Chemistry* 294: 20122-20134

Li S, Shi B, Liu X, An H-X (2020) Acetylation and Deacetylation of DNA Repair Proteins in Cancers. *Frontiers in Oncology* 10

Lin Y-y, Lu J-y, Zhang J, Walter W, Dang W, Wan J, Tao S-C, Qian J, Zhao Y, Boeke JD *et al* (2009) Protein Acetylation Microarray Reveals that NuA4 Controls Key Metabolic Target Regulating Gluconeogenesis. *Cell* 136: 1073-1084

Mahaney BL, Lees-Miller SP, Cobb JA (2014) The C-terminus of Nej1 is critical for nuclear localization and non-homologous end-joining. *DNA Repair* 14: 9-16

Miller KM, Tjeertes JV, Coates J, Legube G, Polo SE, Britton S, Jackson SP (2010) Human HDAC1 and HDAC2 function in the DNA-damage response to promote DNA nonhomologous end-joining. *Nature Structural & Molecular Biology* 17: 1144-1151

Mojumdar A, Sorenson K, Hohl M, Toulouze M, Lees-Miller SP, Dubrana K, Petrini JHJ, Cobb JA (2019) Nej1 Interacts with Mre11 to Regulate Tethering and Dna2 Binding at DNA Double-Strand Breaks. *Cell Reports* 28: 1564-1573.e1563

Noordermeer SM, Adam S, Setiaputra D, Barazas M, Pettitt SJ, Ling AK, Olivieri M, Álvarez-Quilón A, Moatti N, Zimmermann M *et al* (2018) The shieldin complex mediates 53BP1-dependent DNA repair. *Nature* 560: 117-121

Oh J, Al-Zain A, Cannavo E, Cejka P, Symington Lorraine S (2016) Xrs2 Dependent and Independent Functions of the Mre11-Rad50 Complex. *Molecular Cell* 64: 405-415

Ooi SL, Shoemaker DD, Boeke JD (2001) A DNA Microarray-Based Genetic Screen for Nonhomologous End-Joining Mutants in Saccharomyces cerevisiae. *Science* 294: 2552-2556

Orthwein A, Noordermeer SM, Wilson MD, Landry S, Enchev RI, Sherker A, Munro M, Pinder J, Salsman J, Dellaire G *et al* (2015) A mechanism for the suppression of homologous recombination in G1 cells. *Nature* 528: 422-426

Paciotti V, Clerici M, Lucchini G, Longhese MP (2000) The checkpoint protein Ddc2, functionally related to S. pombe Rad26, interacts with Mec1 and is regulated by Mec1-dependent phosphorylation in budding yeast. *Genes & Development* 14: 2046-2059

Reid DA, Keegan S, Leo-Macias A, Watanabe G, Strande NT, Chang HH, Oksuz BA, Fenyo D, Lieber MR, Ramsden DA *et al* (2015) Organization and dynamics of the nonhomologous end-joining machinery during DNA double-strand break repair. *Proceedings of the National Academy of Sciences* 112: E2575-E2584

Rossetto D, Cramet M, Wang AY, Steunou A-L, Lacoste N, Schulze JM, Côté V, Monnet-Saksouk J, Piquet S, Nourani A *et al* (2014) Eaf5/7/3 form a functionally independent NuA4 submodule linked to RNA polymerase II-coupled nucleosome recycling. *The EMBO Journal* 33: 1397-1415

Setiaputra D, Ahmad S, Dalwadi U, Steunou A-L, Lu S, Ross JD, Dong M-Q, Côté J, Yip CK (2018) Molecular Architecture of the Essential Yeast Histone Acetyltransferase Complex NuA4 Redefines Its Multimodularity. *Molecular and Cellular Biology* 38: e00570-00517

Smith GCM, Jackson SP (1999) The DNA-dependent protein kinase. *Genes & Development* 13: 916-934

Sorenson KS, Mahaney BL, Lees-Miller SP, Cobb JA (2017) The non-homologous end-joining factor Nej1 inhibits resection mediated by Dna2–Sgs1 nuclease-helicase at DNA double strand breaks. *Journal of Biological Chemistry* 292: 14576-14586

Soria G, Polo Sophie E, Almouzni G (2012) Prime, Repair, Restore: The Active Role of Chromatin in the DNA Damage Response. *Molecular Cell* 46: 722-734

Steunou A-L, Cramet M, Rossetto D, Aristizabal MJ, Lacoste N, Drouin S, Côté V, Paquet E, Utley RT, Krogan N *et al* (2016) Combined Action of Histone Reader Modules Regulates NuA4 Local Acetyltransferase Function but Not Its Recruitment on the Genome. *Molecular and Cellular Biology* 36: 2768-2781

Steunou A-L, Rossetto D, Côté J (2014) Regulating Chromatin by Histone Acetylation. In: *Fundamentals of Chromatin*, Workman J.L., Abmayr S.M. (eds.) pp. 147-212. Springer New York: New York, NY

Sulek M, Yarrington R, McGibbon G, Boeke JD, Junop M (2007) A critical role for the C-terminus of Nej1 protein in Lif1p association, DNA binding and non-homologous end-joining. *DNA Repair* 6: 1805-1818

Symington LS (2016) Mechanism and regulation of DNA end resection in eukaryotes. *Critical Reviews in Biochemistry and Molecular Biology* 51: 195-212

Tang J, Cho NW, Cui G, Manion EM, Shanbhag NM, Botuyan MV, Mer G, Greenberg RA (2013) Acetylation limits 53BP1 association with damaged chromatin to promote homologous recombination. *Nature Structural & Molecular Biology* 20: 317-325

Trovesi C, Falcettoni M, Lucchini G, Clerici M, Longhese MP (2011) Distinct Cdk1 Requirements during Single-Strand Annealing, Noncrossover, and Crossover Recombination. *PLOS Genetics* 7: e1002263

Tsukamoto Y, Mitsuoka C, Terasawa M, Ogawa H, Ogawa T (2005) Xrs2p Regulates Mre11p Translocation to the Nucleus and Plays a Role in Telomere Elongation and Meiotic Recombination. *Molecular Biology of the Cell* 16: 597-608

Valencia M, Bentele M, Vaze MB, Herrmann G, Kraus E, Lee SE, Schär P, Haber JE (2001) NEJ1 controls non-homologous end joining in Saccharomyces cerevisiae. *Nature* 414: 666-669

Wysocki R, Javaheri A, Allard S, Sha F, Côté J, Kron SJ (2005) Role of Dot1-Dependent Histone H3 Methylation in G₁ and S Phase DNA Damage Checkpoint Functions of Rad9. *Molecular and Cellular Biology* 25: 8430-8443

Yi C, Ma M, Ran L, Zheng J, Tong J, Zhu J, Ma C, Sun Y, Zhang S, Feng W *et al* (2012) Function and Molecular Mechanism of Acetylation in Autophagy Regulation. *Science* 336: 474-477

Zhang Y, Hefferin ML, Chen L, Shim EY, Tseng H-M, Kwon Y, Sung P, Lee SE, Tomkinson AE (2007) Role of Dnl4–Lif1 in nonhomologous end-joining repair complex assembly and suppression of homologous recombination. *Nature Structural & Molecular Biology* 14: 639-646

Zimmermann M, Lottersberger F, Buonomo SB, Sfeir A, de Lange T (2013) 53BP1 Regulates DSB Repair Using Rif1 to Control 5′ End Resection. *Science* 339: 700-704

Zou L, Elledge SJ (2003) Sensing DNA Damage Through ATRIP Recognition of RPA-ssDNA Complexes. *Science* 300: 1542-1548

FIGURE LEGENDS:

Figure 1: NHEJ factors inhibit NuA4 recruitment and end resection at a DSB in G1.

(A) Schematic representation of Fig1B, wild type Rad9 binds to chromatin and inhibits NuA4 from acetylating histones, whereas Rad9 mutants are unable to bind chromatin thus resulting in acetylation of histones by NuA4.

(B) *In vitro* HAT assay showing inhibition of NuA4 acetyltransferase activity by Rad9 using yeast native chromatin and recombinant Rad9 (wild type, tudor-Y798Q and BRCT- K1088E domain mutant). Recombinant Rad9 wild type and mutants were incubated with MMS-treated purified yeast native chromatin. Afterwards NuA4 was added along with ^{3}H-acetyl-CoA followed by spotting on P81 membrane and scintillation counting. Error bars indicate the ranges of duplicate reactions.

(C-H) ChIP-qPCR showing increased recruitment of NuA4(Eaf1 subunit) and Rfa1 (RPA) in *rad9*Δ (C-D)*, yku80*Δ, y*ku80*Δ*rad9*Δ (E-F) and *nej1*Δ (G-H) compared to wild type at an HO-induced DSB in G1. ChIP-qPCR analysis was performed using Eaf1 and Rfa1 antibodies. Cells with *bar1*Δ background were synchronized in G1 phase using α-factor for 6 hours in YP-Raffinose followed by addition of galactose for 3 hours to induce DSB. The data represents two independent biological replicates and error bar denotes range between the replicates. Yeast strains used had similar HO cutting efficiency (Fig EV1D-H)

Figure 2: Xrs2-dependent recruitment of NuA4 at a DSB in G1.

(A-D) ChIP-qPCR of Rfa1 and Eaf1 shows loss of NuA4 (A, C) and resection (B, D) in *xrs2*Δ, *xrs2*Δ*rad9*Δ (A-B) and *xrs2*Δ*rad9*Δy*ku80*Δ (D-E) compared to wild type at HO-induced DSB in G1 synchronized cells.

(E-F) ChIP-qPCR in the *mre11-H125N* mutant shows decreased resection but unaffected NuA4 recruitment compared to wild type in G1 cells. ChIP-qPCR was performed as described in (Fig 1). Yeast strains used showed similar HO cutting efficiency (Fig EV2A-C).

Figure 3: Xrs2-independent and Lcd1-dependent recruitment of NuA4 at DSB.

(A-D) Resection and NuA4 recruitment is restored in *xrs2*Δ background with expression of Mre11-NLS from a low copy number CEN:ARS plasmid. ChIP-qPCR of Eaf1 and Rfa1 was performed as in (Fig 1). (A-B) In G1 cells the increase in NuA4 and Rfa1 is seen in the *rad9*Δy*ku80*Δ background. (C-D) In asynchronous cells; expression of Mre11-NLS is enough to restore NuA4 and Rfa1 levels comparable to WT on the left side proximal to the DSB site.

(E-F) NuA4 recruitment to DSB requires Lcd1. (E) Resection is rescued in *lcd1*Δ*xrs2*Δ+*pMRE11-NLS* with overexpression of Exo1-WT but not Exo1-D173A mutant. (F) NuA4 signal does not show a resection-correlated increase with Exo1-WT compared to the Exo1-D173A mutant or the empty vector. % of Intact DNA was determined by qPCR on genomic DNA at indicated sites and normalized to negative control intergenic V. Cells were grown in YP-Raff till early log phase followed by addition of galactose for 3 hours to induce the DSB. Yeast strains used had similar HO cutting efficiency (Fig EV3B, C, F).

Figure 4: Decreased hyper-resection in *esa1* temperature sensitive mutant in G1.

(A-B) ChIP-qPCR of Rad52 around HO-induced DSB in G1 blocked cells. *rad9*Δy*ku80*Δ, y*ku80*Δ (A) and *nej1*Δ (B) show higher recruitment of Rad52 than compared to wild type.

(C) Reduced histone H4 acetylation in *esa1-ts* background at semi-restrictive temperature. Western blot analysis for WCE of yeast strains used for ChIP-qPCR in (D). Samples were collected before addition of α-factor at permissive temperature (23°C) in YP-Raff. α-factor was added and cultures were moved to semi-restrictive temperature (32°C) followed by addition of galactose to induced DSB for 3 hours.

(D) ChIP-qPCR of Rfa1 around the HO-induced DSB in G1 cells showing reduced resection in *rad9Δyku80Δ* background with the introduction of the *esa1-ts* NuA4 defective allele. Yeast strains used had similar HO cutting efficiency (Fig EV4C).

(E) The sensitivity of the *esa1-ts* mutant cells to DNA damage is partially suppressed by deletion of core NHEJ factors. 10-fold serial dilution spot assays were performed with *esa1-L254P*, *rad9*Δy*ku80*Δ and *rad9*Δy*ku80*Δ*esa1-L254P* cells in the absence or the presence of DNA damaging agent MMS.

Figure 5: NuA4 inhibits NHEJ through acetylation of Nej1.

(A) Western blot on whole cell extracts comparing wild type and mutant Nej1 expression levels in strains used in (B).

(B) *nej1-3KR* and *nej1-3KQ* mutant cells show reduced plasmid re-ligation efficiency for EcoR1 linearized pSO98 plasmid. Samples were normalized to wild type, which was set at 100%.

(C-D) Increased NuA4 and resection/RPA recruitment in the *nej1-3KQ* mutant compared to wild type *NEJ1* and the *nej1-3KR* mutant background. ChIP-qPCR using anti-Eaf1 (D) and anti-Rfa1 (E) antibodies in G1 synchronized cells as described in (Fig 1). Yeast strains used showed similar HO cutting efficiency (Fig EV5C).

(E) Recombinant Nej1-3KQ shows reduced interaction with rKu80 compared to Nej1-WT and Nej1-3KR. rNej1 is GST tagged for pull-down whereas rKu80 is 6X-His tagged. Empty GST was used as negative control.

(F) Recombinant Nej1-3KQ and Nej1-3KR show reduced interaction with rLif1 compared to wild type Nej1. rLif1 is 6X-His tagged. Empty GST was used as negative control.

(G) Ku80 is acetylated on lysine residues *in vivo* in a NuA4-dependent manner. Acetyl-lysine immunoprecipitation in an Esa1-FRB anchor away/Yku80-13myc background shows much reduced signal for Yku80 after the rapamycin treatment that depletes Esa1 from the nucleus. The effect of DNA damage was also monitored by treating the cells with MMS. Pgk1 was used as loading control. The efficiency of Esa1 depletion was monitored by western blot showing loss of H4 acetylation (Fig EV5G).

Figure 6: NuA4 regulates DSB repair pathway choice, favoring resection-based repair.

While chromatin-bound Rad9 can inhibit NuA4-dependent acetylation to favor repair by NHEJ, NuA4 regulates DSB repair pathway choice by acetylating NHEJ core factors like Nej1 and Yku80. This perturbs the interaction between NHEJ factors, enabling resection of DNA ends. As resection produces ssDNA more NuA4 is recruited through its interaction with Lcd1/Ddc2. “Ac” represents acetylation performed by NuA4.

Expanded View Figure Legends:

Figure EV1: NuA4 and resection spreading are not inhibited by NHEJ factors in asynchronous cells.

(A) Purified recombinant Rad9 wild-type and mutants were resolved by SDS-PAGE and stained with Coomassie blue stain. Known concentrations of BSA were used to estimation the concentration of purified recombinant proteins using ImageJ software.

(B) ChIP-qPCR showing NuA4 enrichment around DSB at *MAT* locus between wild type and *rad9*Δ in asynchronous cells.

(C) ChIP-qPCR with antibody against Rfa1 showing no difference in resection at *MAT* locus between wild type and *nej1*Δ in asynchronous cells.

(D-H) HO cutting efficiency at *MAT* locus after 3 hours of galactose induction between wild type and, *rad9*Δ asynchronous cells (C), *rad9*Δ G1 synchronized cells (D), y*ku80*Δ and y*ku80*Δ*rad9*Δ G1 synchronized cells (E), *nej1*Δ G1 synchronized cells (F), *nej1*Δ asynchronous cells (G).

Figure EV2: Difference in NuA4 and resection signal seen between wild type and mutants not caused by uneven HO cutting at *MAT* locus.

(A-C) HO cutting efficiency at MAT locus in G1 synchronized cells after 3 hours of galactose induction between wild type and, *xrs2*Δ*rad9*Δ (A), *xrs2*Δ*rad9*Δy*ku80*Δ (B), *mre11-H125N* (C).

Figure EV3: *MRE11-NLS* suppresses defect of *xrs2*Δ.

(A) Phenotypic analysis showing introduction of *MRE11-NLS* suppresses the sensitivity of *xrs2*Δ to DNA damaging drug, MMS. 1:10 serial dilutions of log phase cells were spotted on synthetic complete -URA plates with and without MMS.

(B-C) HO cutting efficiency at *MAT* locus after 3 hours of galactose induction in the indicated strains.

(D-E) ChIP-qPCR showing *lcd1*Δ *xrs2*Δ results in loss of RPA signal (D), and loss of NuA4 (E) at HO induced DSB at *MAT* locus in asynchronous cells. *lcd1*Δ (loss of Mec1) does not affect resection but shows less signal compared to wild type near the break.

(F) HO cutting efficiency at *MAT* locus after 3 hours of galactose induction in the indicated strains.

Figure EV4: *esa1-ts* does not affect the recruitment of recombination protein in hyper resection background in G1 phase.

(A) ChIP-qPCR with Rad51 antibody around the induced DSB at *MAT* locus in G1 synchronized cells. y*ku80*Δ and y*ku80*Δ*rad9*Δ show higher signal compared to wild type.

(B) ChIP-qPCR with Rad52 antibody around the induced DSB at *MAT* locus in G1 synchronized cells. *rad9Δyku80Δ* and *rad9Δyku80Δesa1-ts* show higher signal for Rad52 than wild type.

(C) HO cutting efficiency in wild type, *rad9Δyku80Δ* and *rad9Δyku80Δesa1-ts* at *MAT* locus in G1 synchronized cells after 3 hours of galactose induction.

Figure EV5: Nej1 mutants do not disrupt DNA damage induced phosphorylation but affect binding to Mre11.

(A) Nej1 is acetylated *in vivo* on residues K18, K192 and K234 in a NuA4-dependent manner. Mass spectrometry analysis of Nej1 lysine acetylation sites in *ESA1* wild type and temperature sensitive (ts) mutant.

(B) Nej1 wild-type and lysine mutants show similar ability to repair chromosomal DSB induced at *MAT* locus by HO induction.

(C) HO cutting efficiency at *MAT* locus in G1 synchronized cells after 3 hours of galactose induction in the indicated *nej1*Δ strains.

(D) *In vitro* protein pull-down assay showing recombinant Nej1 wild type and Nej1-3KR binds to C-terminal of rMre11, while this interaction is much reduced with Nej1-3KQ. Empty GST was used as negative control.

(E) Nej1 lysine mutants do not affect the DNA damage induced phosphorylation of Nej1. Western blot analysis of whole cell extracts (WCE) prepared from indicated yeast strains treated with MMS (0.05%) or DMSO (control) for 2 hours. Pgk1 was used as loading control.

(F) Western blot analysis on WCE showing depletion of Esa1 does not affect the DNA damage induced phosphorylation of Nej1. Esa1 was FRB tagged and depleted from the nucleus using the anchor away system in presence of rapamycin. This was followed by treatment of cells with MMS or DMSO. Pgk1 was used as loading control.

(G) Western blot analysis of yeast WCE showing reduced acetylation of H4 in the anchor away background with Esa1 FRB tagged after rapamycin treatment. H2B was used as loading control.

FIGURE 1

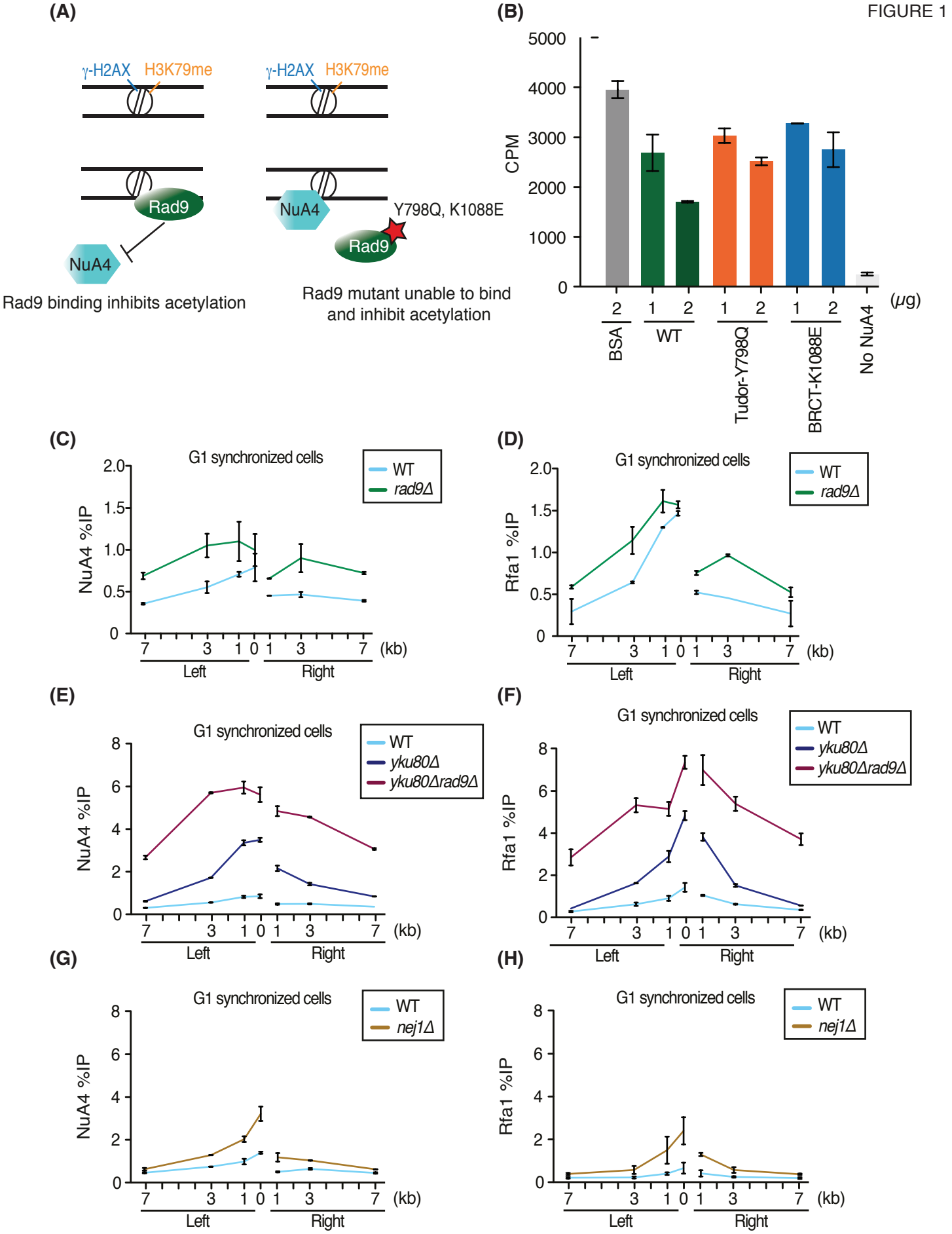
(A)
γ-H2AX
H3K79me
Rad9
NuA4
Rad9 binding inhibits acetylation
γ-H2AX
H3K79me
NuA4
Y798Q, K1088E
Rad9
Rad9 mutant unable to bind and inhibit acetylation
(B)
CPM
5000
4000
3000
2000
1000
0
2 1 2 1 2 1 2
(μg)
BSA
WT
Tudor-Y798Q
BRCT-K1088E
No NuA4
(C)
G1 synchronized cells
WT
rad9Δ
NuA4 %IP
2.0
1.5
1.0
0.5
0
7 3 1 0 1 3 7 (kb)
Left
Right
(D)
G1 synchronized cells
WT
rad9Δ
Rfa1 %IP
2.0
1.5
1.0
0.5
0
7 3 1 0 1 3 7 (kb)
Left
Right
(E)
G1 synchronized cells
WT
yku80Δ
yku80Δrad9Δ
NuA4 %IP
8
6
4
2
0
7 3 1 0 1 3 7 (kb)
Left
Right
(F)
G1 synchronized cells
WT
yku80Δ
yku80Δrad9Δ
Rfa1 %IP
8
6
4
2
0
7 3 1 0 1 3 7 (kb)
Left
Right
(G)
G1 synchronized cells
WT
nej1Δ
NuA4 %IP
8
6
4
2
0
7 3 1 0 1 3 7 (kb)
Left
Right
(H)
G1 synchronized cells
WT
nej1Δ
Rfa1 %IP
8
6
4
2
0
7 3 1 0 1 3 7 (kb)
Left
Right

FIGURE 2

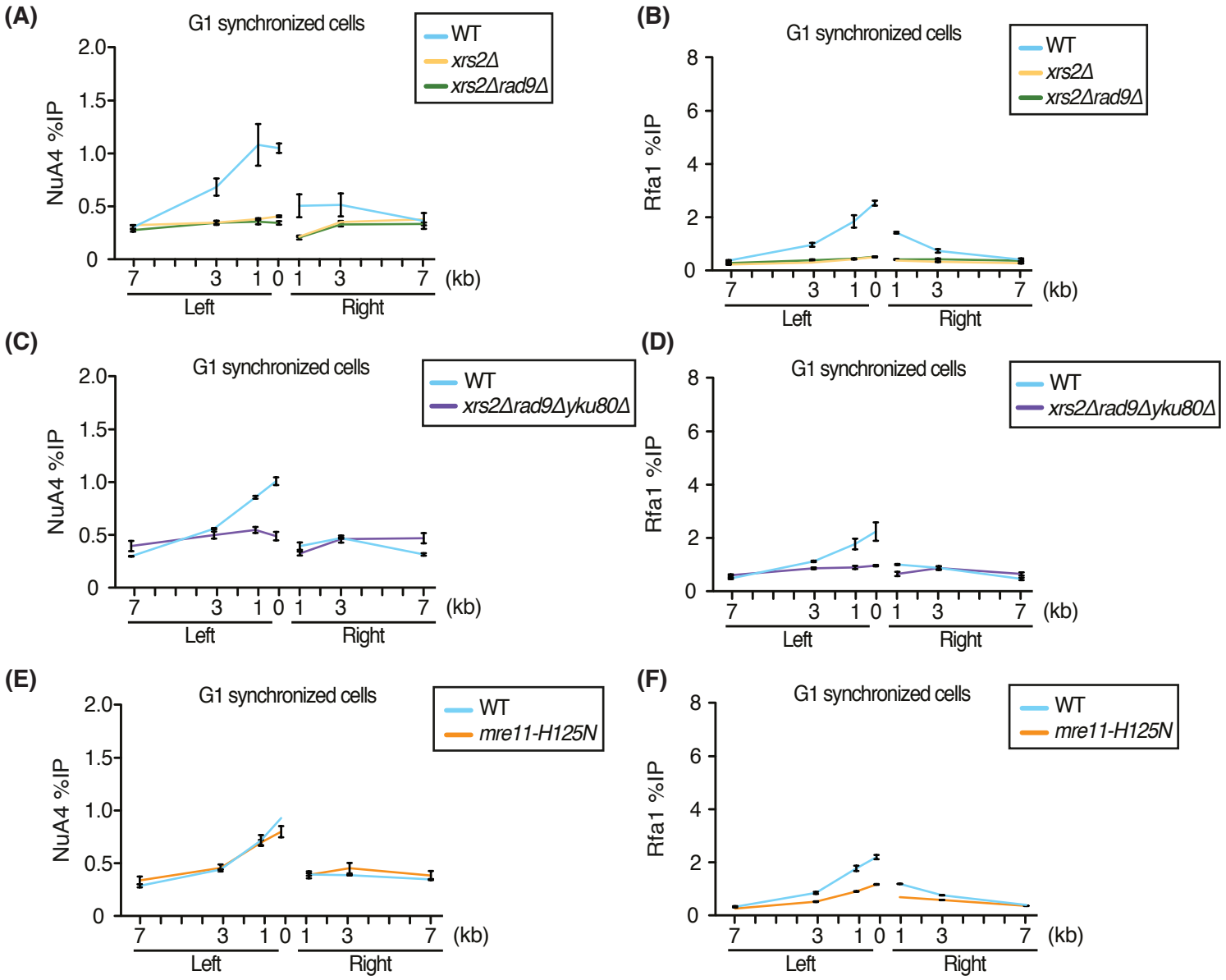
(A)
G1 synchronized cells
WT
xrs2Δ
xrs2Δrad9Δ
NuA4 %IP
2.0
1.5
1.0
0.5
0
7
3
1
0
1
3
7
(kb)
Left
Right
(B)
G1 synchronized cells
WT
xrs2Δ
xrs2Δrad9Δ
Rfa1 %IP
8
6
4
2
0
7
3
1
0
1
3
7
(kb)
Left
Right
(C)
G1 synchronized cells
WT
xrs2Δrad9Δyku80Δ
NuA4 %IP
2.0
1.5
1.0
0.5
0
7
3
1
0
1
3
7
(kb)
Left
Right
(D)
G1 synchronized cells
WT
xrs2Δrad9Δyku80Δ
Rfa1 %IP
8
6
4
2
0
7
3
1
0
1
3
7
(kb)
Left
Right
(E)
G1 synchronized cells
WT
mre11-H125N
NuA4 %IP
2.0
1.5
1.0
0.5
0
7
3
1
0
1
3
7
(kb)
Left
Right
(F)
G1 synchronized cells
WT
mre11-H125N
Rfa1 %IP
8
6
4
2
0
7
3
1
0
1
3
7
(kb)
Left
Right

FIGURE 3

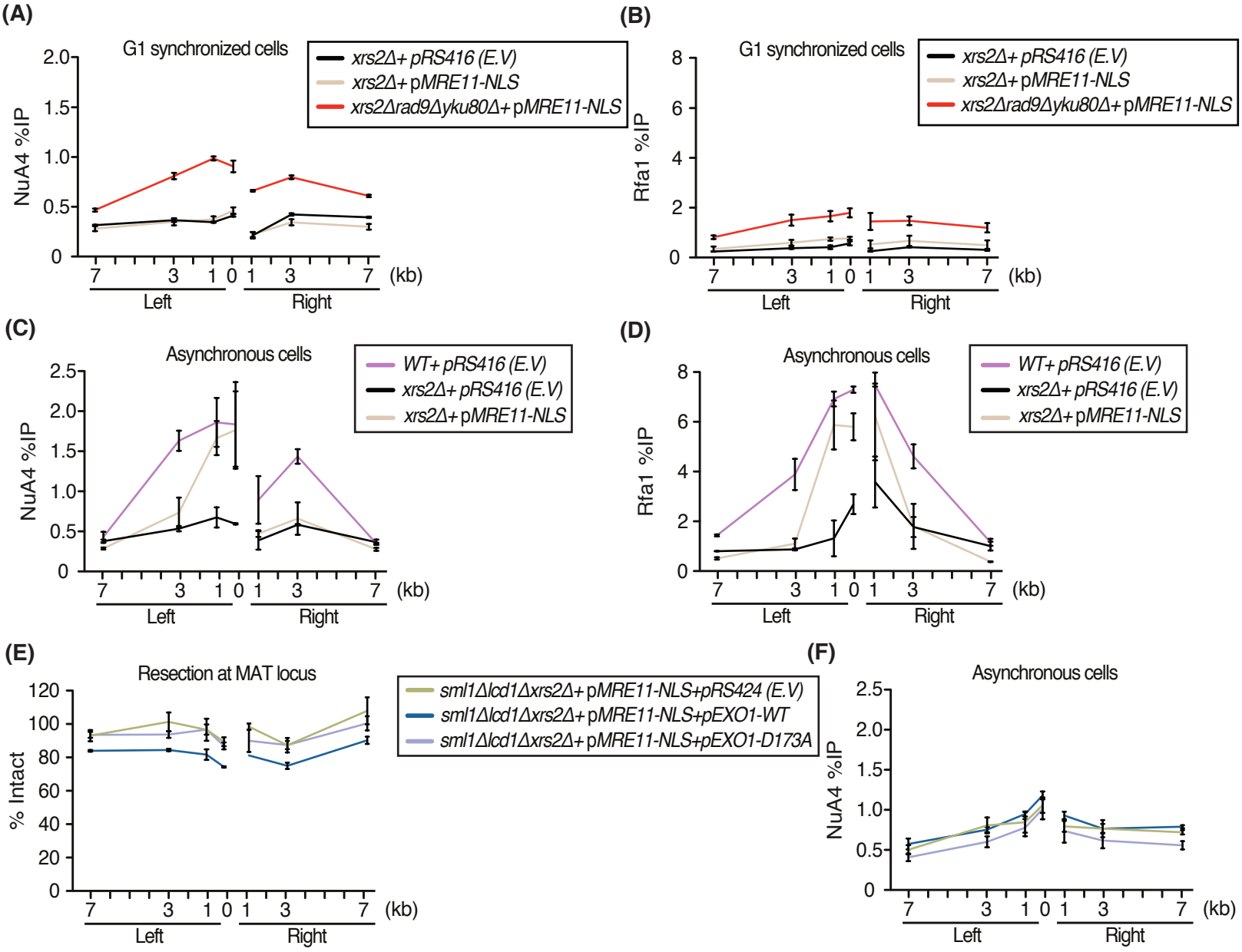
(A)
G1 synchronized cells
xrs2Δ+ pRS416 (E.V)
xrs2Δ+ pMRE11-NLS
xrs2Δrad9Δyku80Δ+ pMRE11-NLS
NuA4 %IP
2.0
1.5
1.0
0.5
0
7 3 1 0 1 3 7 (kb)
Left
Right
(B)
G1 synchronized cells
xrs2Δ+ pRS416 (E.V)
xrs2Δ+ pMRE11-NLS
xrs2Δrad9Δyku80Δ+ pMRE11-NLS
Rfa1 %IP
8
6
4
2
0
7 3 1 0 1 3 7 (kb)
Left
Right
(C)
Asynchronous cells
WT+ pRS416 (E.V)
xrs2Δ+ pRS416 (E.V)
xrs2Δ+ pMRE11-NLS
NuA4 %IP
2.5
2.0
1.5
1.0
0.5
0
7 3 1 0 1 3 7 (kb)
Left
Right
(D)
Asynchronous cells
WT+ pRS416 (E.V)
xrs2Δ+ pRS416 (E.V)
xrs2Δ+ pMRE11-NLS
Rfa1 %IP
8
6
4
2
0
7 3 1 0 1 3 7 (kb)
Left
Right
(E)
Resection at MAT locus
sml1Δlcd1Δxrs2Δ+ pMRE11-NLS+pRS424 (E.V)
sml1Δlcd1Δxrs2Δ+ pMRE11-NLS+pEXO1-WT
sml1Δlcd1Δxrs2Δ+ pMRE11-NLS+pEXO1-D173A
% Intact
120
100
80
60
40
20
0
7 3 1 0 1 3 7 (kb)
Left
Right
(F)
Asynchronous cells
NuA4 %IP
2.5
2.0
1.5
1.0
0.5
0
7 3 1 0 1 3 7 (kb)
Left
Right

FIGURE 4

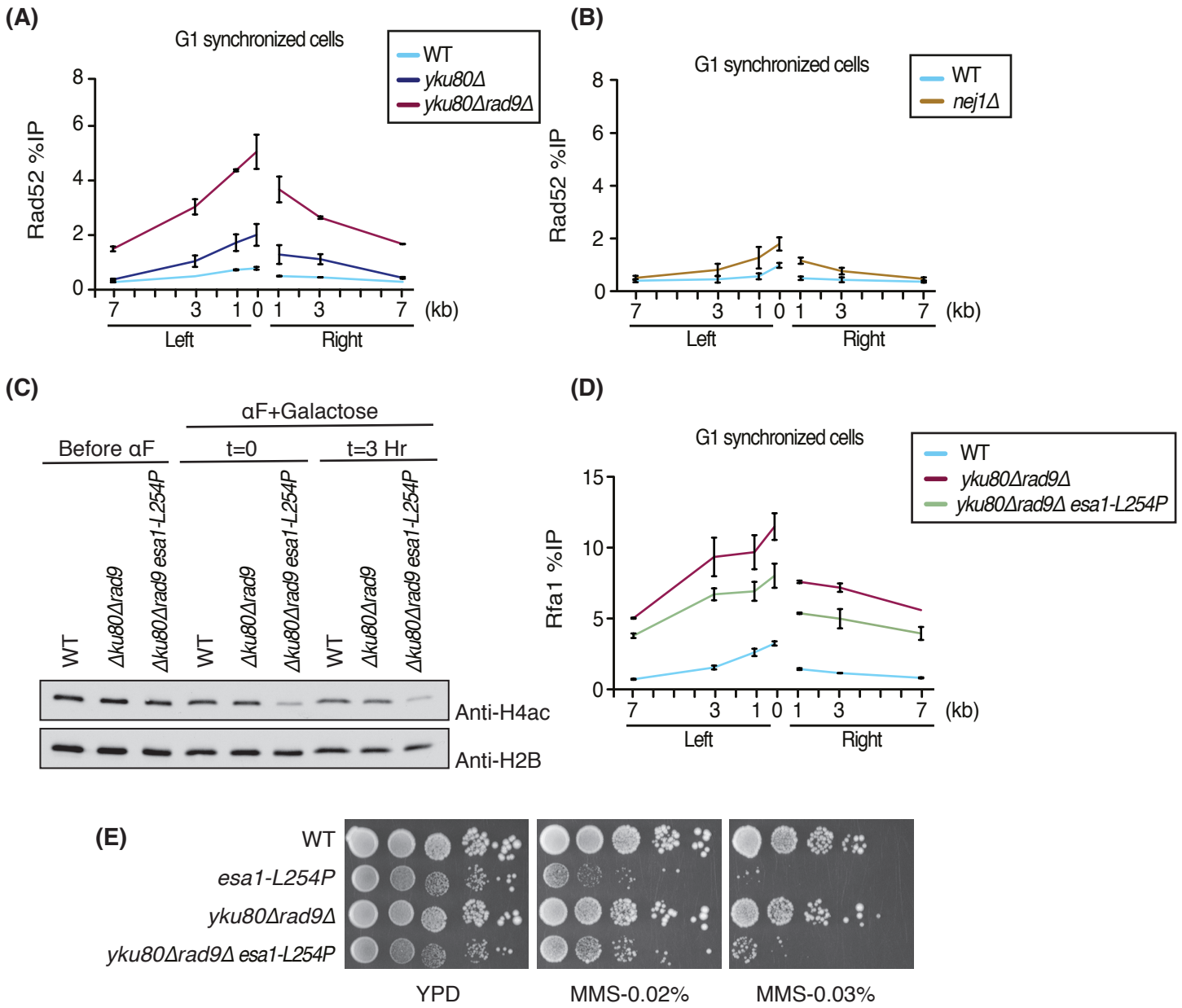
(A)
G1 synchronized cells
WT
yku80Δ
yku80Δrad9Δ
Rad52 %IP
8
6
4
2
0
7
3
1
0
1
3
7
(kb)
Left
Right
(B)
G1 synchronized cells
WT
nej1Δ
Rad52 %IP
8
6
4
2
0
7
3
1
0
1
3
7
(kb)
Left
Right
(C)
αF+Galactose
Before αF
t=0
t=3 Hr
WT
Δku80Δrad9
Δku80Δrad9 esa1-L254P
WT
Δku80Δrad9
Δku80Δrad9 esa1-L254P
WT
Δku80Δrad9
Δku80Δrad9 esa1-L254P
Anti-H4ac
Anti-H2B
(D)
G1 synchronized cells
WT
yku80Δrad9Δ
yku80Δrad9Δ esa1-L254P
Rfa1 %IP
15
10
5
0
7
3
1
0
1
3
7
(kb)
Left
Right
(E)
WT
esa1-L254P
yku80Δrad9Δ
yku80Δrad9Δ esa1-L254P
YPD
MMS-0.02%
MMS-0.03%

FIGURE 5

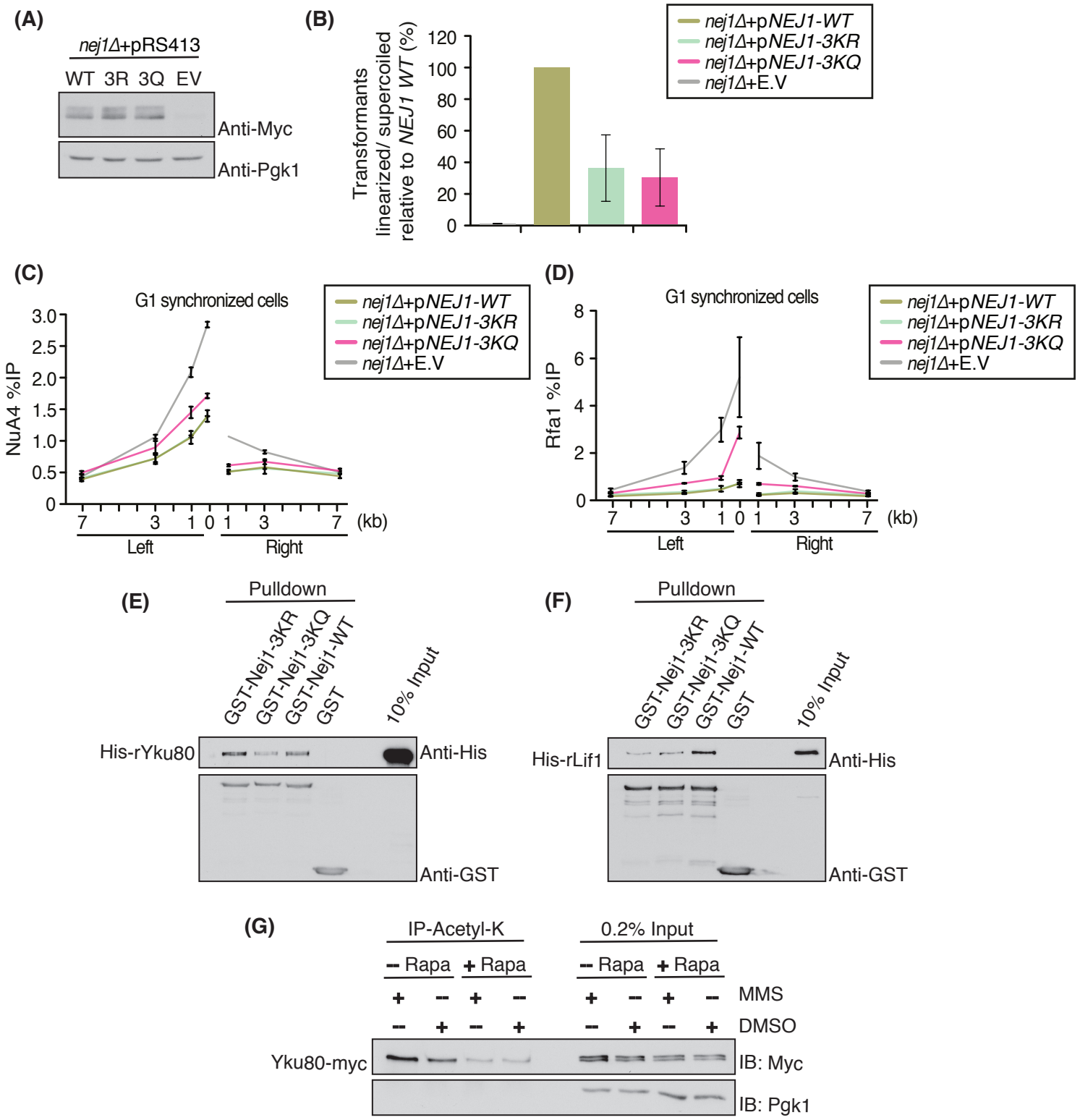
(A)
nej1Δ+pRS413
WT 3R 3Q EV
Anti-Myc
Anti-Pgk1
(B)
Transformants linearized/ supercoiled relative to NEJ1 WT (%)
120
100
80
60
40
20
0
nej1Δ+pNEJ1-WT
nej1Δ+pNEJ1-3KR
nej1Δ+pNEJ1-3KQ
nej1Δ+E.V
(C)
G1 synchronized cells
NuA4 %IP
3.0
2.5
2.0
1.5
1.0
0.5
0
7 3 1 0 1 3 7 (kb)
Left
Right
nej1Δ+pNEJ1-WT
nej1Δ+pNEJ1-3KR
nej1Δ+pNEJ1-3KQ
nej1Δ+E.V
(D)
G1 synchronized cells
Rfa1 %IP
8
6
4
2
0
7 3 1 0 1 3 7 (kb)
Left
Right
nej1Δ+pNEJ1-WT
nej1Δ+pNEJ1-3KR
nej1Δ+pNEJ1-3KQ
nej1Δ+E.V
(E)
Pulldown
GST-Nej1-3KR
GST-Nej1-3KQ
GST-Nej1-WT
GST
10% Input
His-rYku80
Anti-His
Anti-GST
(F)
Pulldown
GST-Nej1-3KR
GST-Nej1-3KQ
GST-Nej1-WT
GST
10% Input
His-rLif1
Anti-His
Anti-GST
(G)
IP-Acetyl-K
0.2% Input
− Rapa + Rapa
− Rapa + Rapa
+ − + − + − + − MMS
− + − + − + − + DMSO
Yku80-myc
IB: Myc
IB: Pgk1

FIGURE 6

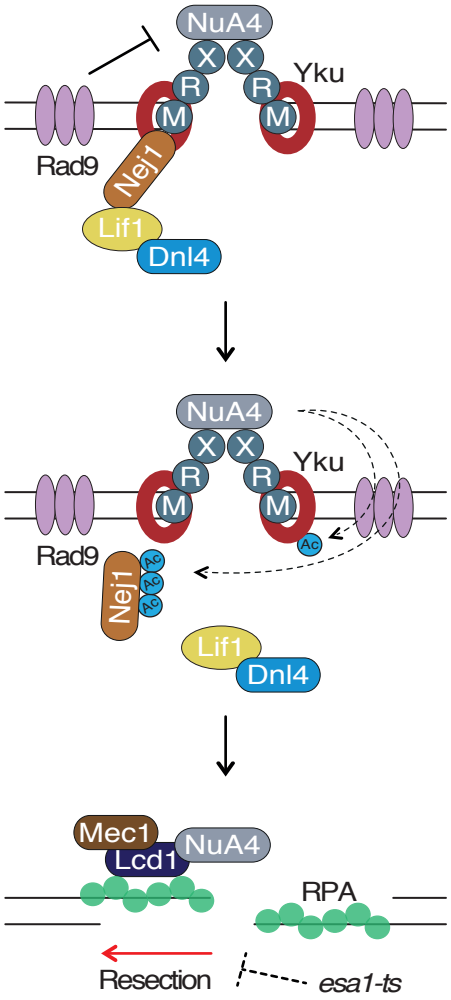
NuA4
X
X
R
R
Yku
M
M
Rad9
Nej1
Lif1
Dnl4
NuA4
X
X
R
R
Yku
M
M
Ac
Rad9
Nej1
Ac
Ac
Ac
Lif1
Dnl4
Mec1
Lcd1
NuA4
RPA
Resection
esa1-ts

FIGURE EV1

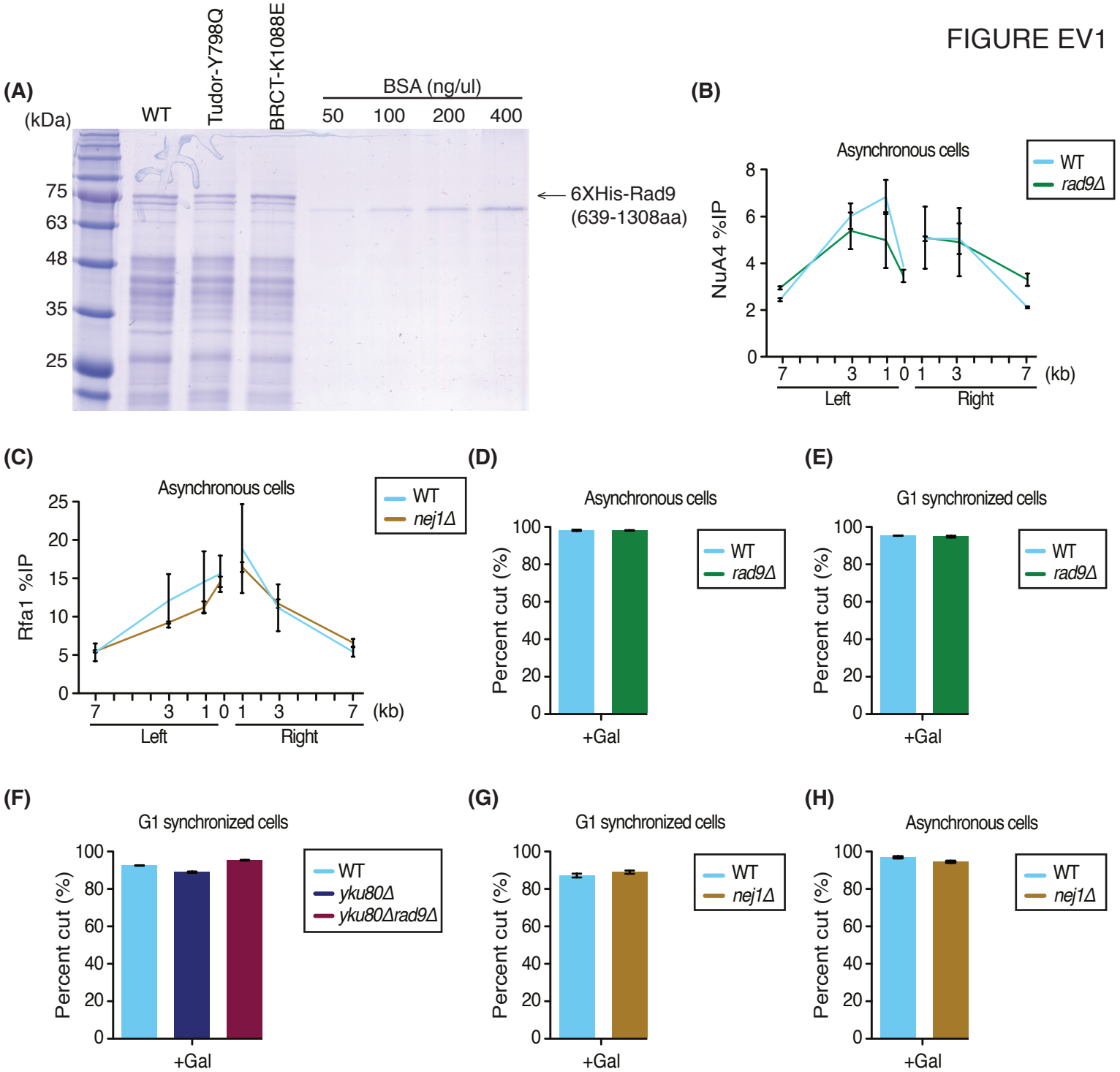
(A)
(kDa)
WT
Tudor-Y798Q
BRCT-K1088E
BSA (ng/ul)
50
100
200
400
75
63
48
35
25
6XHis-Rad9
(639-1308aa)
(B)
Asynchronous cells
WT
rad9Δ
NuA4 %IP
8
6
4
2
0
7
3
1
0
1
3
7
(kb)
Left
Right
(C)
Asynchronous cells
WT
nej1Δ
Rfa1 %IP
25
20
15
10
5
0
7
3
1
0
1
3
7
(kb)
Left
Right
(D)
Asynchronous cells
WT
rad9Δ
Percent cut (%)
100
80
60
40
20
0
+Gal
(E)
G1 synchronized cells
WT
rad9Δ
Percent cut (%)
100
80
60
40
20
0
+Gal
(F)
G1 synchronized cells
WT
yku80Δ
yku80Δrad9Δ
Percent cut (%)
100
80
60
40
20
0
+Gal
(G)
G1 synchronized cells
WT
nej1Δ
Percent cut (%)
100
80
60
40
20
0
+Gal
(H)
Asynchronous cells
WT
nej1Δ
Percent cut (%)
100
80
60
40
20
0
+Gal

FIGURE EV2

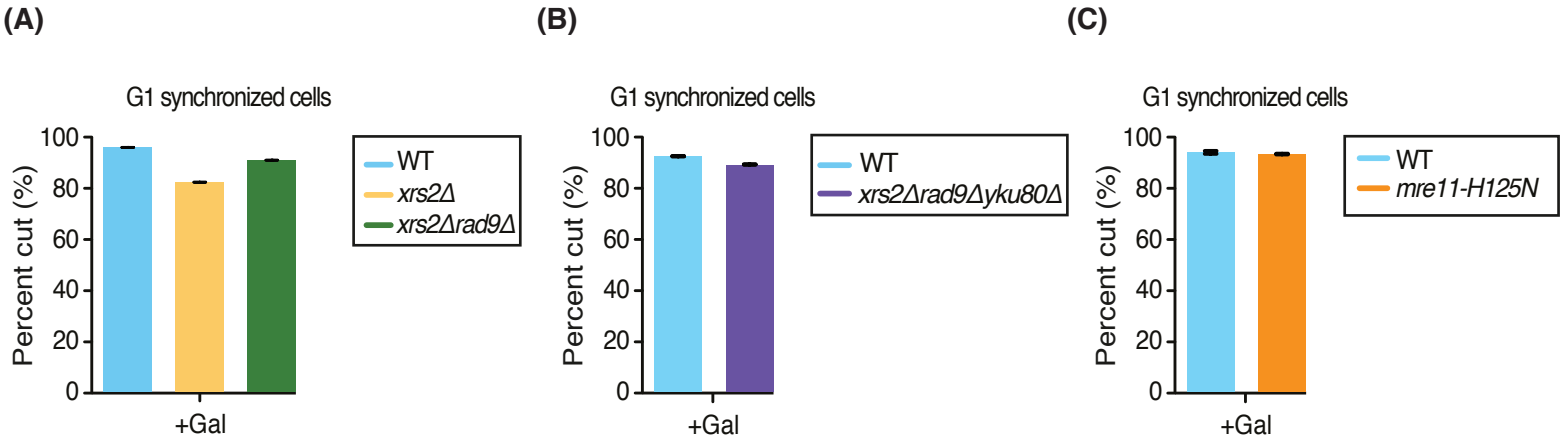
(A)
G1 synchronized cells
Percent cut (%)
100
80
60
40
20
0
+Gal
WT
xrs2Δ
xrs2Δrad9Δ
(B)
G1 synchronized cells
Percent cut (%)
100
80
60
40
20
0
+Gal
WT
xrs2Δrad9Δyku80Δ
(C)
G1 synchronized cells
Percent cut (%)
100
80
60
40
20
0
+Gal
WT
mre11-H125N

FIGURE EV3

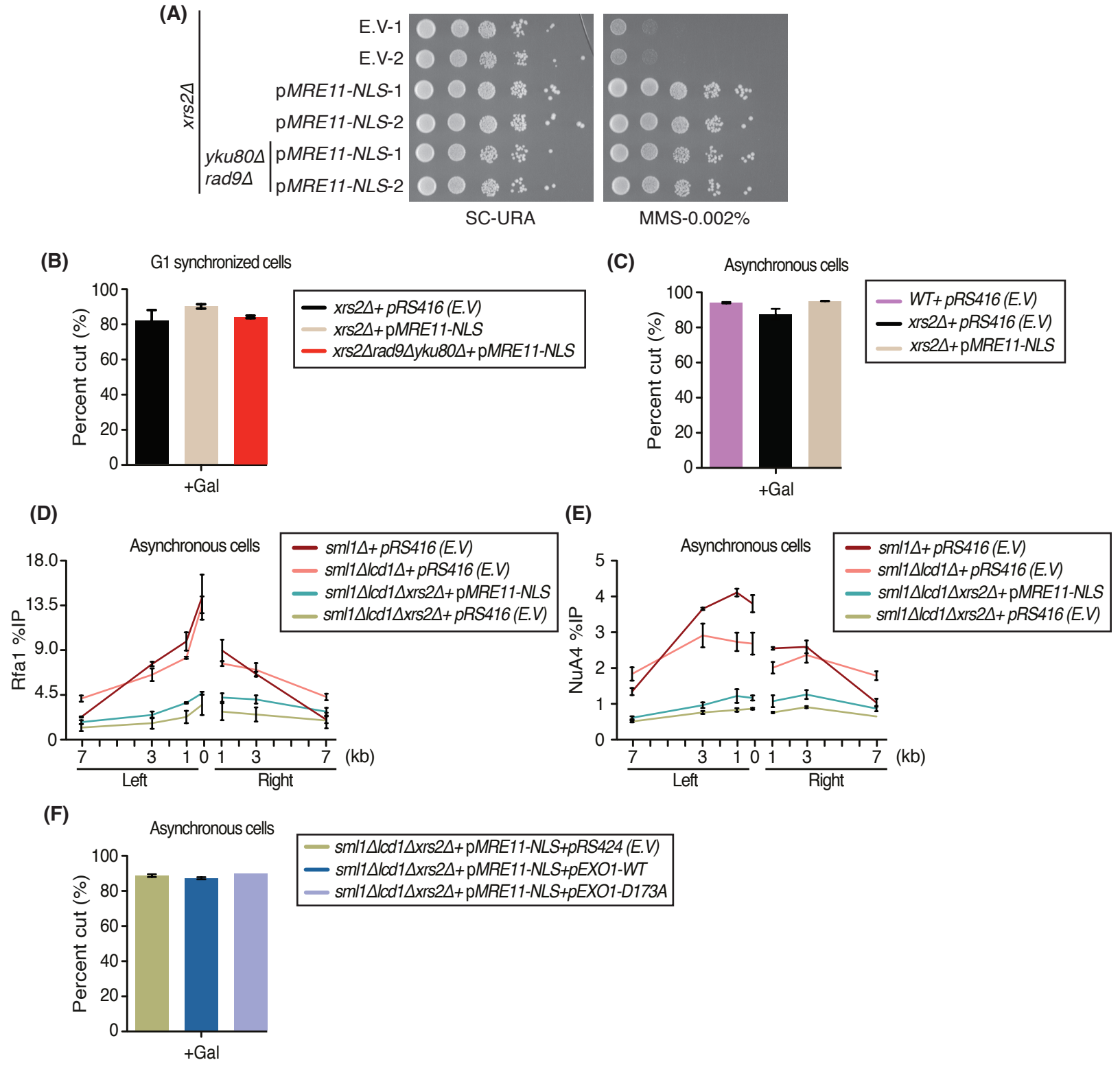
(A)
xrs2Δ
E.V-1
E.V-2
pMRE11-NLS-1
pMRE11-NLS-2
yku80Δ rad9Δ
pMRE11-NLS-1
pMRE11-NLS-2
SC-URA
MMS-0.002%
(B)
G1 synchronized cells
Percent cut (%)
+Gal
xrs2Δ+ pRS416 (E.V)
xrs2Δ+ pMRE11-NLS
xrs2Δrad9Δyku80Δ+ pMRE11-NLS
(C)
Asynchronous cells
Percent cut (%)
+Gal
WT+ pRS416 (E.V)
xrs2Δ+ pRS416 (E.V)
xrs2Δ+ pMRE11-NLS
(D)
Asynchronous cells
Rfa1 %IP
sml1Δ+ pRS416 (E.V)
sml1Δlcd1Δ+ pRS416 (E.V)
sml1Δlcd1Δxrs2Δ+ pMRE11-NLS
sml1Δlcd1Δxrs2Δ+ pRS416 (E.V)
Left
Right
(kb)
(E)
Asynchronous cells
NuA4 %IP
sml1Δ+ pRS416 (E.V)
sml1Δlcd1Δ+ pRS416 (E.V)
sml1Δlcd1Δxrs2Δ+ pMRE11-NLS
sml1Δlcd1Δxrs2Δ+ pRS416 (E.V)
Left
Right
(kb)
(F)
Asynchronous cells
Percent cut (%)
+Gal
sml1Δlcd1Δxrs2Δ+ pMRE11-NLS+pRS424 (E.V)
sml1Δlcd1Δxrs2Δ+ pMRE11-NLS+pEXO1-WT
sml1Δlcd1Δxrs2Δ+ pMRE11-NLS+pEXO1-D173A

FIGURE EV4

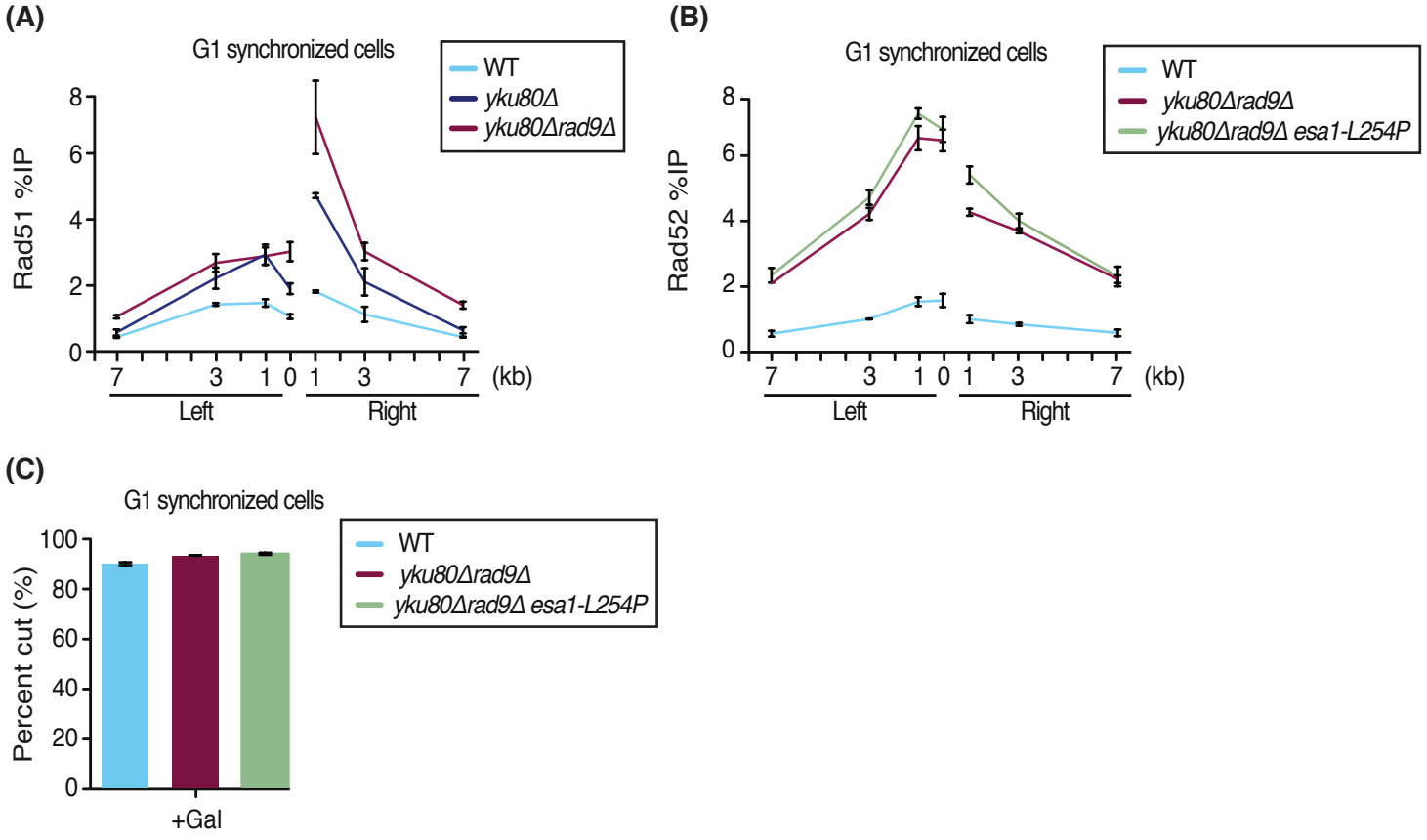
(A)
G1 synchronized cells
WT
yku80Δ
yku80Δrad9Δ
Rad51 %IP
8
6
4
2
0
7
3
1
0
1
3
7
(kb)
Left
Right
(B)
G1 synchronized cells
WT
yku80Δrad9Δ
yku80Δrad9Δ esa1-L254P
Rad52 %IP
8
6
4
2
0
7
3
1
0
1
3
7
(kb)
Left
Right
(C)
G1 synchronized cells
WT
yku80Δrad9Δ
yku80Δrad9Δ esa1-L254P
Percent cut (%)
100
80
60
40
20
0
+Gal

FIGURE EV5

(A)

Ac-Nej1	
Esa1-WT	*esa1-ts*
K18	
K164	K164
K192	
K207	K207
K214	K214
K234	
K317	K317

(B)

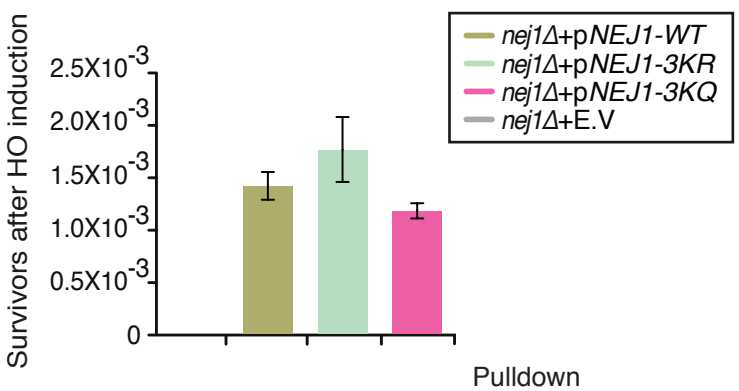

(C)

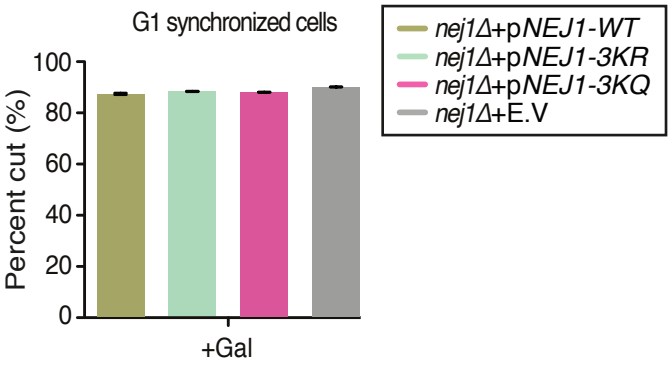

(D)

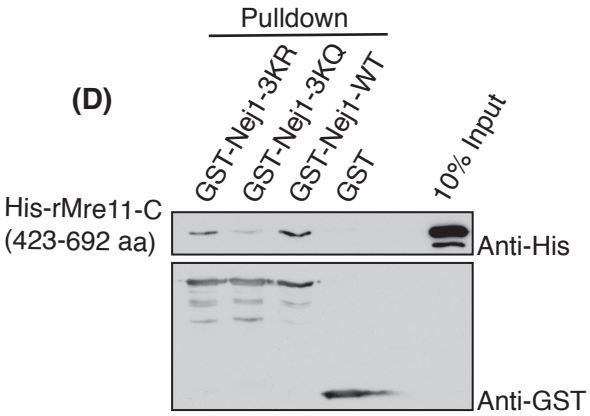

(E)

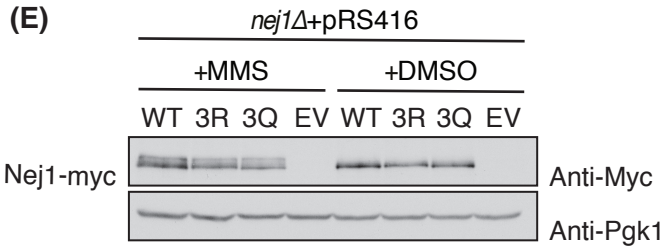

(F)

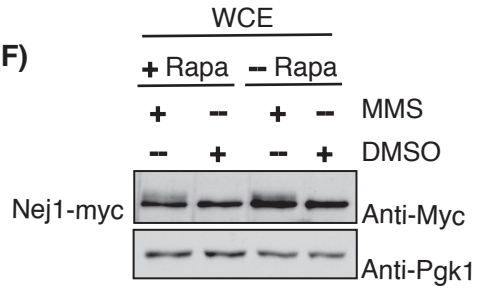

(G)

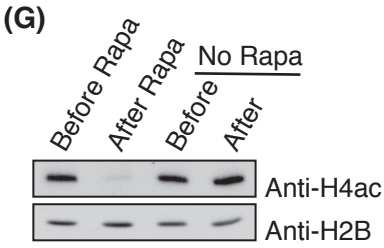

Appendix Table of Contents

Appendix Table S1: Yeast strains used in the current study……P1

Appendix Table S1

Strain	Genotype	Reference
JKM139	*MATa hoΔ hmlΔ::ADE1 hmrΔ::ADE1 ade1-100 leu2-3;112 lys5 trp1::hisG ura3-52 ade3::GAL-HO*	(Lee *et al*, 1998)
QY2211	JKM139 *bar1Δ::NATMX*	This study
QY2212	JKM139 *bar1Δ::NATMX rad9Δ::KANMX*	This study
QY2213	JKM139 *bar1Δ::NATMX yku80Δ*::*TRP1*	This study
QY2214	JKM139 *bar1Δ::NATMX rad9Δ::KANMX yku80Δ*::*TRP1*	This study
QY2231	JKM139 *bar1Δ::LEU2 rad9Δ::KANMX yku80Δ*::*TRP1 esa1-L254P::NATMX*	This study
QY2215	JKM139 *bar1Δ::NATMX nej1Δ*::*TRP1*	This study
QY2216	JKM139 *bar1Δ::NATMX xrs2Δ*::*TRP1*	This study
QY2217	JKM139 *bar1Δ::NATMX rad9Δ::KANMX xrs2Δ*::*TRP1*	This study
QY2218	JKM139 *bar1Δ::NATMX rad9Δ::KANMX xrs2Δ*::*TRP1 yku80Δ*::*HPHMX*	This study
QY2219	JKM139 *bar1Δ::NATMX mre11-H125N::HPHMX*	This study
QY2220	JKM139 *bar1Δ::NATMX* + (pRS416)	This study
QY2221	JKM139 *bar1Δ::NATMX xrs2Δ*::*TRP1* + (pRS416)	This study
QY2222	JKM139 *bar1Δ::NATMX xrs2Δ*::*TRP1* + (pRS416 *MRE11-NLS*)	This study
QY2223	JKM139 *bar1Δ::NATMX rad9Δ::KANMX xrs2Δ*::*TRP1 yku80Δ*::*HPHMX* + (pRS416 *MRE11-NLS*)	This study
QY1603	JKM139 *sml1::NATMX*	(Cheng *et al.*, 2018)
QY1604	JKM139 *sml1::NATMX lcd1::KANMX*	(Cheng *et al.*, 2018)
QY2224	QY1603 + (pRS416)	This study
QY2225	QY1604 + (pRS416)	This study
QY-2226	QY1604 *xrs2Δ::LEU2* + (pRS416)	This study
QY2227	QY1604 *xrs2Δ::LEU2* + (pRS416 *MRE11-NLS*)	This study
QY2228	QY2227 + (pRS424 *TRP1 2μ ori*)	This study
QY2229	QY2227 + (pRS424 *EXO1 TRP1 2μ ori*)	This study
QY2230	QY2227 + (pRS424 *EXO1-D173A TRP1 2μ ori*)	This study
QY2600	BY4741 *MATa his3Δ1 leu2Δ0 met15Δ0 ura3Δ0 nej1Δ*::*KANMX*	This study
QY2232	QY2600 + (pRS413)	This study
QY2233	QY2600 + (pRS413 *NEJ1*)	This study
QY2234	QY2600 + (pRS413 *NEJ1-K18R-K192R-K234R*)	This study
QY2235	QY2600 + (pRS413 *NEJ1-K18Q-K192Q-K234Q*)	This study
QY2236	QY2215 + (pRS416)	This study
QY2237	QY2215 + (pRS416 *NEJ1*)	This study
QY2238	QY2215 + (pRS416 *NEJ1-K18R-K192R-K234R*)	This study
QY2239	QY2215 + (pRS416 *NEJ1-K18Q-K192Q-K234Q)*	This study

QY3572	JKM139 *fpr1Δ::HphMX tor1-1::URA3 RPL13A-2*FKBP12::TRP1 FRB-ESA1::KanMX*	(Kollenstart *et al.*, 2019)
QY2240	QY3572 *YKU80-13MYC::NATMX*	This study
QY2241	QY3572 *NEJ1-13MYC::NATMX*	This study
QY2054	BY4741 *MATa his3Δ1 leu2Δ0 met15Δ0 ura3Δ0* +pEGH(GAL-GST-Nej1)	Open Biosystem
QY2058	BY4741 *MATa his3Δ1 leu2Δ0 met15Δ0 ura3Δ0 esa1Δ::KanMX* +pSAPE5(HA-*esa1-L254P LEU2 ARS/CEN*) +pEGH(GAL-GST-Nej1)	This study